

## CHAPTER 1

### SPACETIME APPROACH TO PHASE TRANSITIONS

Wolfhard Janke

*Institut für Theoretische Physik, Universität Leipzig, Augustusplatz 10/11,  
04109 Leipzig, Germany*

Adriaan M. J. Schakel

*Institut für Theoretische Physik, Freie Universität Berlin, Arnimallee 14, 14195  
Berlin, Germany*

In these notes, the application of Feynman's sum-over-paths approach to thermal phase transitions is discussed. The paradigm of such a spacetime approach to critical phenomena is provided by the high-temperature expansion of spin models. This expansion, known as the hopping expansion in the context of lattice field theory, yields a geometric description of the phase transition in these models, with the thermal critical exponents being determined by the fractal structure of the high-temperature graphs. The graphs percolate at the thermal critical point and can be studied using purely geometrical observables known from percolation theory. Besides the phase transition in spin models and in the closely related  $\phi^4$  theory, other transitions discussed from this perspective include Bose-Einstein condensation, and the transitions in the Higgs model and the pure U(1) gauge theory.

#### 1. Introduction

Feynman's spacetime approach to quantum mechanics provides a marvelously intuitive, yet computationally powerful entry to the quantum world.<sup>1</sup> In this sum-over-paths approach, transition amplitudes are computed by summing over all possible trajectories a particle can take. Although it is most extensively applied to nonrelativistic quantum mechanics,<sup>2</sup> for which it was originally designed, the worldline approach also found applications in the context of relativistic systems.<sup>3,4</sup> (For overviews and references to a host of applications in high energy physics,

see Refs. [5, 6, 7, 8].) In these notes, we explore its use in the theory of critical phenomena.

The possibility to adapt Feynman's sum-over-paths approach to describe phase transitions derives from particle-field duality. Featuring the particle content of the system, the spacetime approach provides a completely equivalent alternative to the quantum field theoretic description. Although by no means the only successful method,<sup>9</sup> field theory is frequently used to describe critical phenomena,<sup>10,11,12</sup> whether the fluctuations are thermal as in phase transitions taking place at finite temperature, or quantum as in zero-temperature transitions. Particle-field duality then opens the possibility for a spacetime approach to critical phenomena. In the context of classical critical phenomena, the line objects described by the field theory are current lines.

Though not formulated as such, the high-temperature expansion of spin models<sup>13,6</sup> probably provides the first example of the spacetime approach to critical phenomena (see below). A particular intuitive example is offered by the nonlinear  $O(N)$  spin model defined on a lattice in the limit  $N \rightarrow 0$ , where the high-temperature graphs form random self-avoiding walks.<sup>14</sup> In the early 1950ies, Feynman<sup>15</sup> applied his approach to the superfluid phase transition in liquid  $^4\text{He}$ , and showed that, in this picture, Bose-Einstein condensation arises when the worldlines of individual particles combine to form large lines threading the entire system. In the late 1970ies,<sup>16,17,18,19,20</sup> the approach was applied to phase transitions in relativistic lattice models possessing line-like topological defects, thus mapping these models onto the statistical mechanics problem of random loop configurations. The line defects were pictured as forming a grand canonical ensemble of fluctuation loops of arbitrary shape and length—a so-called *loop gas*. In the 1980ies, the statistical properties of such loop gases were further investigated in the context of cosmic strings and their role in phase transitions in the early universe, with the loop distribution given a central position,<sup>21,22</sup> as well as in the context of deconfinement phase transitions, where percolation observables were introduced to characterize them.<sup>23,24</sup> More recently, these ideas were pursued further with the goal to arrive at a complete quantitative understanding of phase transitions in terms of the geometrical properties of the loop gas under consideration.<sup>25,26,27,28,29,30,31,32</sup> The resulting geometric description of critical phenomena ties together various strains of theoretical physics: statistical mechanics, quantum field theory, polymer physics, and percolation theory—all to be discussed below.

The plan of these notes is as follows. In Sec. 2, the particle content of

the linear  $O(N)$  symmetric quantum field theory, defined on a hypercubic lattice, is studied in the spirit of Feynman's sum-over-paths approach, starting from the noninteracting theory in Secs. 2.1 and 2.2. Interactions are perturbatively included in Sec. 2.3, where also the spacetime interpretation of Feynman diagrams is pursued. In Sec. 2.4, the strong-coupling limit, where the field theory reduces to the nonlinear  $O(N)$  spin model, is considered. The high-temperature representation of the nonlinear model is shown to provide a purely geometric representation, directly connected to Feynman's spacetime approach for the linear model. As a case study, the high-temperature representation of the Ising model, corresponding to  $N = 1$ , on a square lattice is detailed in Sec. 2.5.

In Sec. 3, the critical properties of the  $O(N)$  universality class are examined from the perspective of particle trajectories or high-temperature graphs. In Sec. 3.1, their fractal structure is investigated, while in Sec. 3.2, the proliferation of these lines is shown to drive the  $O(N)$  phase transition. In Sec. 3.3, the fractal structure of the worldlines or high-temperature graphs is related to the critical behavior. The general relations are first applied to self-avoiding random walks, corresponding to the  $N \rightarrow 0$  limit, in two dimensions (Sec. 3.4), and to arbitrary  $-2 \leq N \leq 2$  (Sec. 3.5) also in two dimensions, where many exact results are available for comparison.

In Sec. 4, the high-temperature representation of the Ising model is investigated by means of Monte Carlo simulations. The Metropolis update used to generate the high-temperature graphs is introduced in Sec. 4.1, while the numerical results are summarized in Sec. 4.2.

In Sec. 5, the conclusions for the  $O(N)$  universality class are extended to charged systems (Sec. 5.1) and to Bose-Einstein condensation (Sec. 5.2) to demonstrate the generality of the spacetime approach to phase transitions.

Finally, in Sec. 6, the worldlines or high-temperature graphs are reinterpreted as line defects in two (Sec. 6.1), three (Sec. 6.2), and four (Sec. 6.3) dimensions, respectively, and the so-called dual field theories, which feature these line-like configurations as topological defects, briefly discussed.

## 2. Lattice Field Theory

Central to our discussion is the  $O(N)$  symmetric relativistic quantum field theory formulated on a hypercubic lattice in  $d$  Euclidean spacetime dimensions, with the time coordinate analytically continued to the imaginary axis  $\tau$ . As an illustration, the cubic lattice in Fig. 1 represents discretized spacetime in one time and two space dimensions  $x_1$  and  $x_2$ . The theory,

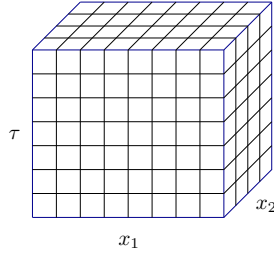


Fig. 1. Cubic lattice representing three-dimensional discretized spacetime.

describing self-interacting scalar particles of mass  $m$ , is specified by the (Euclidean) partition function

$$Z = \text{Tr} e^{-S}, \quad (1)$$

where  $S$  is the lattice action

$$S = a^d \sum_x \left[ \frac{1}{2a^2} \sum_{\mu} (\varphi_{x+a\hat{\mu}} - \varphi_x)^2 + \frac{m^2}{2} \varphi_x^2 + \frac{g}{4!} \varphi_x^4 \right], \quad (2)$$

with  $g$  the coupling constant and  $a$  the lattice spacing. The real scalar field  $\varphi_x$  defined on each lattice site  $x$  of the spacetime box has  $N$  components  $\varphi_x = \varphi_x^\alpha = (\varphi_x^1, \varphi_x^2, \dots, \varphi_x^N)$ , with the index  $\alpha = 1, 2, \dots, N$  labeling the field components and  $\varphi_x^4 \equiv (\varphi_x \cdot \varphi_x)^2$ , where the dot product implies a summation over the field components  $\varphi_x \cdot \varphi_x = \sum_{\alpha=1}^N \varphi_x^\alpha \varphi_x^\alpha$ . Lattice coordinates, representing discretized spacetime, are specified by  $x = x_\mu = (x_1, x_2, \dots, x_d)$ , with  $\mu = 1, 2, \dots, d$  and  $x_d = \tau$  denoting the imaginary time coordinate, while  $\hat{\mu}$  denotes the unit vector pointing in the  $\mu$ -direction. In the continuum limit  $a \rightarrow 0$ , the lattice action reduces to

$$S = \int d^d x \left\{ \frac{1}{2} [\partial_\mu \varphi(x)]^2 + \frac{m^2}{2} \varphi^2(x) + \frac{g}{4!} \varphi^4(x) \right\}, \quad (3)$$

where  $\varphi(x)$  stands for the field defined in continuous spacetime. Unless otherwise indicated, natural units  $\hbar = c = 1$  are adopted throughout. The trace  $\text{Tr}$  in Eq. (1) stands for the sum or integral over all possible field configurations:

$$\text{Tr} = \prod_x \int d\varphi_x. \quad (4)$$

In the continuum limit, where the lattice spacing is taken to zero  $a \rightarrow 0$ , the right hand defines the *functional* measure denoted by  $\int D\varphi$ .

For numerical simulations, a more convenient form of the lattice action is obtained by casting Eq. (2) in terms of dimensionless fields and parameters defined via<sup>33</sup>

$$a^{d-2}\varphi_x^2 = 2K\phi_n^2 \quad (5)$$

$$a^{4-d}g = 6\frac{\lambda}{K^2} \quad (6)$$

$$m^2a^2 = \frac{1-2\lambda N}{K} - 2d. \quad (7)$$

The action then takes the form of an  $O(N)$  spin model

$$S = -K \sum_{\langle n, n' \rangle} \phi_n \cdot \phi_{n'} + \sum_n \phi_n^2 + \lambda \sum_n (\phi_n^2 - N)^2. \quad (8)$$

Each site on the hypercubic spacetime lattice is now specified by the vector  $n = n_\mu = (n_1, n_2, \dots, n_d)$  with integer components  $n_\mu = x_\mu/a$  and the sum  $\sum_{\langle n, n' \rangle}$  extends over all nearest neighbor pairs. In terms of these new dimensionless variables, the action is independent of the lattice spacing  $a$ . The partition function  $Z$  now reads

$$Z = \int D\mu(\phi) \exp \left( K \sum_{\langle n, n' \rangle} \phi_n \cdot \phi_{n'} \right), \quad (9)$$

with the on-site measure

$$\int D\mu(\phi) = \int \prod_n d\phi_n e^{-\phi_n^2 - \lambda(\phi_n^2 - N)^2}. \quad (10)$$

In the limit  $\lambda \rightarrow \infty$ , the field theory reduces to the standard  $O(N)$  spin model, with a “spin” variable  $\phi_n$  of fixed length,  $\phi_n^2 = N$ , located at each site of the spacetime lattice.

### 2.1. Noninteracting Theory

We first consider the limit  $\lambda \rightarrow 0$  in Eq. (8), corresponding to the noninteracting field theory. The rescaling factor  $K$  introduced in Eqs. (5)-(7) then becomes

$$K = \frac{1}{2d + m^2a^2} \quad (11)$$

and the action reduces to the quadratic form

$$S_0 = \sum_{n, n'} \phi_n \cdot \Lambda_{n, n'} \phi_{n'}, \quad (12)$$

with

$$\Lambda_{n,n'} = \delta_{n,n'} - K \sum_{\pm\mu} \delta_{n,n'+\hat{\mu}} \quad (13)$$

where the sum  $\sum_{\pm\mu}$  extends over the positive as well as the negative directions. In matrix notation

$$\Lambda = I - K H, \quad (14)$$

where  $I$  is the identity matrix and  $H$  denotes the so-called hopping matrix whose elements  $H_{n,n'}$  are unity if the two lattice sites  $n$  and  $n'$  are nearest neighbors, and zero otherwise. Physically,  $H$  describes the hopping, or propagation of a particle from one lattice site, representing a spacetime cell, to an adjacent one, with each hop carrying a weight  $K$ . Since the theory is noninteracting, a particle is free to hop at random to any of its nearest neighbors without restriction. It can and will in general revisit sites previously visited and can even hop onto a site already occupied by another particle. The particle trajectories are therefore *phantom* worldlines that can freely intersect and share bonds of the lattice without energy penalty.

The inverse of  $\Lambda$  determines the lattice correlation function:

$$\langle \phi_n^\alpha \phi_{n'}^\beta \rangle = \frac{1}{2} \delta_{\alpha,\beta} \Lambda_{n,n'}^{-1} = \frac{1}{2} \delta_{\alpha,\beta} \sum_{b=0}^{\infty} H_{n,n'}^b K^b, \quad (15)$$

as can be read off from the action (12). From the definition of the hopping matrix  $H$  it follows that  $H_{n,n'}$  raised to the power  $b$  gives the number of paths  $z_b(n, n')$  of  $b$  steps starting at site  $n$  and ending at site  $n'$ . In this so-called *hopping expansion*,<sup>34</sup> the correlation function is therefore obtained by summing over all possible worldlines of arbitrary many steps joining the endpoints  $n$  and  $n'$ .<sup>35</sup>

$$\langle \phi_n^\alpha \phi_{n'}^\beta \rangle = \frac{1}{2} \delta_{\alpha,\beta} \sum_{b=0}^{\infty} z_b(n, n') K^b = \frac{1}{2} \delta_{\alpha,\beta} \sum_{\text{worldlines}} K^b. \quad (16)$$

Each path carries a weight  $K^b$  according to the number of steps  $b$  taken. This geometric representation of the correlation function as a sum over worldlines constitutes Feynman's spacetime approach<sup>1</sup> to fluctuating fields on the lattice. The equivalence of the two approaches is known as *particle-field duality*.

Because of translational invariance, the number of particle trajectories  $z_b(n, n')$  depends only on the relative coordinate  $z_b(n, n') = z_b(n - n')$ . It

satisfies the recurrence relation

$$z_{b+1}(n) = \sum_{\pm\mu} z_b(n + \hat{\mu}), \quad (17)$$

with the initial condition  $z_0(n) = \delta_{0,n}$ . This relation is easily solved by going over to Fourier space

$$z_b(n - n') = \int_{-\pi}^{\pi} \frac{d^d q}{(2\pi)^d} e^{iq \cdot (n - n')} z_b(q), \quad (18)$$

with  $q \cdot n = q_\mu n_\mu = q_1 n_1 + \cdots q_d n_d$  and  $q_\mu$  the dimensionless momentum variable, yielding

$$z_{b+1}(q) = \sum_{\mu} \cos(q_\mu) z_b(q). \quad (19)$$

With  $z_0(q) = 1$  as initial condition, this gives for  $z_b(n - n')$

$$z_b(n - n') = \int_{-\pi}^{\pi} \frac{d^d q}{(2\pi)^d} e^{iq \cdot (n - n')} \left[ 2 \sum_{\mu} \cos(q_\mu) \right]^b. \quad (20)$$

In the limit where the lattice spacing  $a$  is small but still finite, so that the particles still take discrete steps, we have

$$\begin{aligned} \left[ 2K \sum_{\mu} \cos(q_\mu) \right]^b &\rightarrow \left( \frac{1 - q^2/2d}{1 + m^2 a^2/2d} \right)^b \\ &\rightarrow \exp \left[ -(q^2 + m^2 a^2)b/2d \right]. \end{aligned} \quad (21)$$

The lattice correlation function (16) then becomes

$$\begin{aligned} \langle \phi_n^\alpha \phi_{n'}^\beta \rangle &\rightarrow \delta_{\alpha,\beta} \frac{1}{2} \sum_{b=0}^{\infty} \int_{-\pi}^{\pi} \frac{d^d q}{(2\pi)^d} e^{iq \cdot (n - n')} e^{-(q^2 + m^2 a^2)b/2d} \\ &\rightarrow \delta_{\alpha,\beta} \frac{1}{2} \sum_{b=1}^{\infty} \left( \frac{d}{2\pi b} \right)^{d/2} \exp \left[ -\frac{d(n - n')^2}{2b} \right] e^{-m^2 a^2 b/2d}, \end{aligned} \quad (22)$$

showing that the end-to-end vector  $n - n'$  is Gaussian distributed with an extra Boltzmann weight  $\exp(-m^2 a^2/2d)$  associated with each step taken. Because of this bond fugacity, long worldlines are exponentially suppressed as long as the mass term in the action is positive,  $m^2 > 0$ . Notice that in the last line of Eq. (22), the lower bound on the summation is replaced by  $b = 1$ . This is justified because the  $b = 0$  term always vanishes for  $n \neq n'$ .

A more familiar expression for the correlation function is obtained from Eq. (16) by first summing over the length  $b$  of the particle trajectories. With  $z_b(n, n')$  given in Eq. (20), this leads to

$$\begin{aligned} \langle \phi_n^\alpha \phi_{n'}^\beta \rangle &= \delta_{\alpha, \beta} \frac{1}{2} \int_{-\pi}^{\pi} \frac{d^d q}{(2\pi)^d} \frac{e^{iq \cdot (n-n')}}{1 - 2K \sum_{\mu} \cos(q_{\mu})} \\ &= \delta_{\alpha, \beta} \frac{1}{2K} \int_{-\pi}^{\pi} \frac{d^d q}{(2\pi)^d} \frac{e^{iq \cdot (n-n')}}{2 \sum_{\mu} [1 - \cos(q_{\mu})] + m^2 a^2}. \end{aligned} \quad (23)$$

For the original fields  $\varphi_x$ , which are connected to the rescaled fields  $\phi_n$  through Eq. (5), this translates into the standard form of the correlation function of a free field theory on a hypercubic lattice,

$$\langle \varphi_x^\alpha \varphi_{x'}^\beta \rangle = \delta_{\alpha, \beta} a^2 \int_{-\pi/a}^{\pi/a} \frac{d^d k}{(2\pi)^d} \frac{e^{ik \cdot (x-x')}}{2 \sum_{\mu} [1 - \cos(k_{\mu} a)] + m^2 a^2}, \quad (24)$$

where the lattice sites are now labeled again by  $x_{\mu} = n_{\mu} a$ , and  $k_{\mu} = q_{\mu}/a$  is the momentum variable.

In the limit  $a \rightarrow 0$ , the correlation function (24) reduces to the standard continuum expression

$$\langle \varphi_x^\alpha \varphi_{x'}^\beta \rangle = \delta_{\alpha, \beta} \int_{-\infty}^{\infty} \frac{d^d k}{(2\pi)^d} \frac{e^{ik \cdot (x-x')}}{k^2 + m^2}. \quad (25)$$

The momentum integral can be easily carried out by introducing the Schwinger proper time representation<sup>4</sup> of the integrand, which is based on Euler's form

$$\frac{1}{A^z} = \frac{1}{\Gamma(z)} \int_0^{\infty} \frac{ds}{s} s^z e^{-sA}, \quad (26)$$

where  $\Gamma(z)$  is the Euler gamma function. Specifically,

$$\begin{aligned} \langle \varphi_x^\alpha \varphi_{x'}^\beta \rangle &= \delta_{\alpha, \beta} \int_0^{\infty} ds \int \frac{d^d k}{(2\pi)^d} e^{ik \cdot (x-x')} e^{-s(k^2 + m^2)} \\ &= \delta_{\alpha, \beta} \int_0^{\infty} ds \left( \frac{1}{4\pi s} \right)^{d/2} e^{-(x-x')^2/4s} e^{-sm^2} \\ &= \delta_{\alpha, \beta} \frac{1}{(2\pi)^{d/2}} \left( \frac{m}{|x-x'|} \right)^{d/2-1} K_{d/2-1}(m|x-x'|), \end{aligned} \quad (27)$$

with  $K_{d/2-1}$  a modified Bessel function. The integral in the second line is the continuum limit of the lattice expression (22), with the sum over the number of steps  $b$  taken by the particle replaced by an integral over the Schwinger proper time parameter  $s$ , with the identification

$$ba^2/2d \equiv s. \quad (28)$$



The parameter  $s$  is related to the proper time  $\tau_p$  of the trajectory traced out by the point particle, for which

$$\left(\frac{dx_\mu(\tau_p)}{d\tau_p}\right)^2 = 1. \quad (29)$$

To make this evident, we write the integrand in the second line of Eq. (27) as a Feynman path integral<sup>19</sup>

$$\begin{aligned} & \left(\frac{1}{4\pi s}\right)^{d/2} e^{-(x-x')^2/4s} e^{-sm^2} \\ &= \int_{x(0)=x}^{x(s)=x'} Dx(s') \exp\left\{-\int_0^s ds' \left[\frac{1}{4}\dot{x}^2(s') + m^2\right]\right\}, \end{aligned} \quad (30)$$

where the so-called Wiener measure is defined by

$$\int_{x(0)=x}^{x(s)=x'} Dx(s') \equiv \lim_{b \rightarrow \infty} A^b \prod_{i=1}^{b-1} \int_{-\infty}^{\infty} dx_i, \quad (31)$$

with the normalization factor

$$A = \left(\frac{d}{2\pi a^2}\right)^{d/2}. \quad (32)$$

Here, it is understood that the limit  $b \rightarrow \infty$  is taken concurrently with the continuum limit  $a \rightarrow 0$  in a way such that  $ba^2 \rightarrow \text{const}$ . The classical action of the point particle in Eq. (30), tracing out its trajectory in spacetime is the continuum limit of the lattice action present in Eq. (22):

$$\begin{aligned} W_0 &= \frac{d}{2} \sum_{i=1}^b \left(\frac{x_{i-1} - x_i}{a}\right)^2 + \frac{m^2 a^2 b}{2d} \\ &= \sum_{i=1}^b \frac{a^2}{2d} \left[\frac{1}{4} \left(\frac{x_{i-1} - x_i}{a^2/2d}\right)^2 + m^2\right] \\ &\rightarrow \int_0^s ds' \left[\frac{1}{4}\dot{x}^2(s') + m^2\right], \end{aligned} \quad (33)$$

where in the last step the identification (28) is used. Written as a path integral, the correlation function (27) thus reads

$$\langle \varphi_x^\alpha \varphi_{x'}^\beta \rangle = \delta_{\alpha,\beta} \int_0^\infty ds \int_{x(0)=x}^{x(s)=x'} Dx(s') e^{-W_0}. \quad (34)$$

It forms the continuum limit of the sum over all possible particle trajectories on the spacetime lattice in Eq. (16). Note that the proper time parameter

$s$  can take any positive value, in agreement with the lattice representation (16) of the correlation function where the worldlines can be arbitrary long. The Boltzmann factor  $\exp(-sm^2)$  exponentially suppresses, however, large proper times as long as  $m^2 > 0$ . When we set

$$s \equiv \tau_p/2m, \quad (35)$$

the continuum action (33) yields  $m$  times the arc length of the path,

$$\int_0^s ds' \left[ \frac{1}{4} \dot{x}^2(s') + m^2 \right] = m\tau_p, \quad (36)$$

which is the standard form of the classical action of a relativistic free scalar particle of mass  $m$ . This demonstrates that  $s$  can indeed be thought of as the proper time.

For later use, we record the second line in Eq. (27) with Planck's constant and the speed of light reinstalled:

$$\left\langle \varphi_x^\alpha \varphi_0^\beta \right\rangle = \delta_{\alpha,\beta} c \int_0^\infty ds \left( \frac{1}{4\pi\hbar s} \right)^{d/2} e^{-(c^2\tau^2 + \mathbf{x}^2)/4\hbar s} e^{-sm^2c^2/\hbar}, \quad (37)$$

while the continuum action (3) becomes

$$S_0 = \int d\tau d^{d-1}x \varphi \left( -\hbar^2 \frac{\partial^2}{c^2 \partial \tau^2} - \hbar^2 \nabla^2 + m^2 c^2 \right) \varphi, \quad (38)$$

where now the spacetime coordinates are denoted by  $x_\mu = (\mathbf{x}, c\tau)$ , with  $\tau$  the imaginary time and  $\mathbf{x} = (x_1, \dots, x_{d-1})$  the spatial coordinates.

Besides the number of worldlines  $z_b(n, n')$  on the spacetime lattice connecting the lattice sites  $n$  and  $n'$  in  $b$  steps, also the probability  $P_b(n, n')$  for a particle to move from  $n$  to  $n'$  in  $b$  steps will become important below. The probability is given by the ratio

$$P_b(n, n') = z_b(n, n')/z_b \quad (39)$$

of  $z_b(n, n')$  and the number of paths of  $b$  steps starting at  $n$  and ending at an arbitrary lattice site,

$$z_b \equiv \sum_{n'} z_b(n, n'). \quad (40)$$

The denominator in Eq. (39) is included so that  $P_b$  is a genuine probability, taking values between 0 and 1. To evaluate it, imagine the particle taking a first step to one of its nearest neighbors  $n \pm \hat{\mu}$ . It then has only  $n-1$  steps still

available to reach the final destination  $n'$  with probability  $P_{b-1}(n \pm \hat{\mu}, n')$ . That is,  $P_b$  satisfies the recurrence relation:

$$P_b(n, n') = \frac{1}{2d} \sum_{\pm\mu} P_{b-1}(n + \hat{\mu}, n') \quad (41)$$

where the factor  $2d$  denotes the number of nearest neighbors on a  $d$ -dimensional square lattice. When  $P_{b-1}(n, n')$  is subtracted from both sides of Eq. (41), the difference equation

$$P_b(n, n') - P_{b-1}(n, n') = \frac{1}{2d} \sum_{\pm\mu} [P_{b-1}(n + \hat{\mu}, n') - P_{b-1}(n, n')] \quad (42)$$

follows, with the boundary condition  $P_0(n, n') = \delta_{n, n'}$ . As before, the continuum limit is taken by simultaneously letting  $a \rightarrow 0$  and  $b \rightarrow \infty$ , such that  $ba^2 \rightarrow \text{const}$ . The difference equation then turns into the differential equation

$$\partial_b P_b(n, n') = \frac{a^2}{2d} \nabla^2 P_b(n, n'), \quad (43)$$

with the celebrated solution

$$P_b(n, n') = \left( \frac{d}{2\pi b} \right)^{d/2} \exp \left[ -\frac{d}{2} \frac{(n - n')^2}{b} \right]. \quad (44)$$

For the probability density  $p_b(x, x') \equiv P_b(n, n')/a^d$  this gives the Gaussian distribution

$$p_b(x, x') = \left( \frac{d}{2\pi ba^2} \right)^{d/2} \exp \left[ -\frac{d}{2} \frac{(x - x')^2}{ba^2} \right]. \quad (45)$$

Each dimension the particle is free to roam contributes a factor  $\sqrt{d/2\pi ba^2}$  to the prefactor.

## 2.2. Loop Gas

A similar geometric representation in terms of particle trajectories as found for the correlation function can be given for the partition function. Consider the partition function of the free theory:

$$Z_0 = \prod_n \int d\phi_n e^{-S_0}, \quad (46)$$

with the lattice action  $S_0$  given by Eq. (12). This integral generalizes the standard Gaussian integral

$$\int \prod_{i=1}^n dx_i \exp \left( -\frac{1}{2} \sum_{i,j=1}^n x_i M_{ij} x_j \right) = (2\pi)^{n/2} \det^{-1/2}(M), \quad (47)$$

with  $M$  a symmetric positive-definite  $n \times n$  matrix, and  $\det(M)$  its determinant. It can therefore be evaluated exactly, with the result

$$\ln Z_0 = \ln \text{Det}^{-N/2}(\Lambda) = -\frac{N}{2} \text{Tr} \ln \Lambda, \quad (48)$$

where  $\text{Tr}$  denotes the functional trace. In deriving this, irrelevant prefactors are ignored and use is made of the identity

$$\ln \text{Det}(A) = \text{Tr} \ln A, \quad (49)$$

relating the determinant and trace of an Hermitian operator  $A$ . The relation can be easily checked explicitly for a  $n \times n$  matrix. With  $\Lambda = I - KH$  as before,  $\ln Z_0$  can be expanded in the hopping parameter  $K$  as

$$\ln Z_0 = \frac{N}{2} L^d \sum_{b=1}^{\infty} \frac{1}{b} z_b(a) K^b \quad (50)$$

where  $z_b(a)$  denotes the number of worldlines of  $b$  steps, starting at a given lattice site  $n$  and returning to one of its nearest neighbor sites  $n \pm \hat{\mu}$  after  $b$  steps (see Fig. 2). The lattice spacing  $a$  serves here as a microscopic cutoff, so that  $z_b(a)$  rather than  $z_b(0)$  appears when closing open paths. Since a worldline can start at any site on the spacetime lattice, the right hand contains a factor  $L^d$ , denoting the total number of lattice sites, and  $\ln Z_0$  is extensive. The factor  $1/2b$  appearing in Eq. (50) reflects the possibility to trace out a closed path starting from any site along the path and going in either direction round it. The factor  $N$  reflects the degeneracy associated with a closed worldline. Written as a sum over *single* loops of arbitrary length and shape, Eq. (50) reads

$$\ln Z_0 = N \sum_{\substack{\text{single} \\ \text{loops}}} K^b, \quad (51)$$

where the loops are considered to have no orientation, whence the absence of the factor  $\frac{1}{2}$ , and no longer rooted, whence the absence of the factor  $L^d$ .

For a noninteracting theory,  $z_b(a)$  can be obtained simply from Eq. (20) by putting the end-to-end vector  $n - n'$  to zero there. Equation (50) then

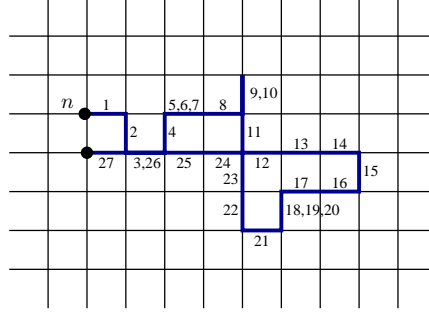


Fig. 2. A Brownian random walk on a square lattice returning to a site adjacent to its starting position  $n$ . As indicated, the particle took 27 steps in total. Observe that various bonds are traversed more than once.

reads explicitly

$$\ln Z_0 = \frac{N}{2} L^d \int_{-\pi}^{\pi} \frac{d^d q}{(2\pi)^d} \sum_{b=1}^{\infty} \frac{1}{b} \left[ 2K \sum_{\mu} \cos(q_{\mu}) \right]^b. \quad (52)$$

Repeating the same steps leading to Eq. (22), one finds

$$\begin{aligned} \ln Z_0 &= \frac{N}{2} L^d \sum_{b=1}^{\infty} \int_{-\pi}^{\pi} \frac{d^d q}{(2\pi)^d} \frac{1}{b} e^{-(q^2 + m^2 a^2) b / 2d} \\ &= \frac{N}{2} L^d \sum_{b=1}^{\infty} \frac{1}{b} \left( \frac{d}{2\pi b} \right)^{d/2} e^{-m^2 a^2 b / 2d}. \end{aligned} \quad (53)$$

It follows that the logarithm of the partition function has the form<sup>21,22</sup>

$$\ln Z_0 \sim \sum_b \ell_b, \quad (54)$$

with the loop distribution

$$\ell_b \sim b^{-\tau} e^{-\theta b}. \quad (55)$$

denoting the average number (per lattice site) of times a closed worldline of  $b$  steps occurs on the lattice. The parameter  $\theta \propto m^2$  physically determines the line tension of the loops, while the algebraic factor in the loop distribution, characterized by the exponent  $\tau = d/2 + 1$ , is an entropy factor, giving a measure of the number of ways a loop of  $b$  steps can be embedded in the lattice.

A more familiar expression for  $\ln Z_0$  is obtained by again first carrying out the sum over the loop length  $b$  in Eq. (52):

$$\begin{aligned}\ln Z_0 &= -\frac{N}{2} L^d \int_{-\pi}^{\pi} \frac{d^d q}{(2\pi)^d} \ln \left[ 1 - 2K \sum_{\mu} \cos(q_{\mu}) \right] \\ &= -\frac{N}{2} \Omega \int_{-\pi/a}^{\pi/a} \frac{d^d k}{(2\pi)^d} \ln \left\{ 2 \sum_{\mu} [1 - \cos(k_{\mu} a)] + m^2 a^2 \right\}, \quad (56)\end{aligned}$$

where in the last step an irrelevant additive factor is ignored and  $\Omega = (La)^d$  is the volume of the spacetime box. This is the standard representation of the logarithm of the partition function describing a free field theory on a hypercubic lattice. In the continuum limit  $a \rightarrow 0$ , the momentum integral can again best be carried out by using the Schwinger proper time representation this time of the logarithm,

$$\ln(a) = \lim_{z \rightarrow 0} \frac{1}{z} - \int_0^{\infty} \frac{ds}{s} e^{-sa}, \quad (57)$$

where the first term is an irrelevant diverging contribution. Apart from further irrelevant additive constants this leads to

$$\begin{aligned}\ln Z_0 &= \ln \text{Det}^{-N/2} (-\partial_{\mu}^2 + m^2) \\ &= -\frac{N}{2} \Omega \int_{-\infty}^{\infty} \frac{d^d k}{(2\pi)^d} \ln(k^2 + m^2) \\ &= \frac{N}{2} \Omega \int_0^{\infty} \frac{ds}{s} \left( \frac{1}{4\pi s} \right)^{d/2} e^{-sm^2}, \quad (58)\end{aligned}$$

where the operator  $-\partial_{\mu}^2 + m^2$  is the continuum limit of  $\Lambda$  introduced in Eq. (13). The right hand of Eq. (58) forms the continuum limit of the lattice expression in the last line of Eq. (53) with the number of steps  $b$  taken by the particle assuming the role of the Schwinger proper time parameter  $s$ :  $ba^2/2d \equiv s$  as in Eq. (28).

On account of the path integral (30) with  $x = x'$ , the last two factors in the integrand at the right hand of Eq. (58) can be written as a path integral over *closed* worldlines

$$e^{-sm^2} \left( \frac{1}{4\pi s} \right)^{d/2} = \oint Dx(s') \exp \left\{ - \int_0^s ds' \left[ \frac{1}{4} \dot{x}^2(s') + m^2 \right] \right\}, \quad (59)$$

where the notation  $\oint Dx(s')$  refers to closed paths. In this way,  $\ln Z_0$  ex-

pressed as a path integral reads<sup>19</sup>

$$\begin{aligned} \ln Z_0 &= \ln \text{Det}^{-N/2} (-\partial_\mu^2 + m^2) \\ &= \frac{N}{2} \Omega \int_0^\infty \frac{ds}{s} \oint Dx(s') \exp \left\{ - \int_0^s ds' \left[ \frac{1}{4} \dot{x}^2(s') + m^2 \right] \right\}, \end{aligned} \quad (60)$$

where the argument of the exponential function is given by (minus) the classical action (33) of the point particle tracing out its trajectories in spacetime. An easy mnemonic for remembering the main ingredients of this formula is to interpret  $-\partial_\mu^2 + m^2$  as the Hamilton operator describing the motion of a *nonrelativistic* particle of mass  $M = \frac{1}{2}$  in a constant potential  $V = m^2$  in  $d$  dimensions. With the Schwinger proper time  $s$  interpreted as Newtonian time,  $W_0$  is the corresponding nonrelativistic action, where it is recalled that in natural units  $\hbar = 1$ .

The first line in Eq. (58) is sometimes represented by the one-loop Feynman diagram

$$\ln Z_0 = \bigcirc. \quad (61)$$

In the spacetime approach, this diagram stands for all the terms in the sum (50), each consisting of a *single* worldline starting and ending at a given site  $n$ . That is, the Feynman diagram at the same time denotes the topology of the particle trajectories contributing to  $\ln Z_0$ .<sup>34</sup>

The partition function, obtained by exponentiating Eq. (50), can be written in terms of Feynman diagrams as

$$Z_0 = 1 + \bigcirc + \frac{1}{2!} \bigcirc \bigcirc + \frac{1}{3!} \bigcirc \bigcirc \bigcirc + \dots \quad (62)$$

Each diagram involves a separate integration over loop momentum  $k_\mu$ . With the right hand of Eq. (62) taken as picturing the topology of the particle trajectories contributing to the partition function, it follows that  $Z_0$  describes a loop gas—a grand canonical ensemble of fluctuation loops of arbitrary shape and length.<sup>20</sup> Being a noninteracting theory, the closed worldlines can freely intersect themselves or other worldlines and even share bonds. On the spacetime lattice, the loop gas (62) can be expressed as a sum over all possible tangles of closed paths

$$Z_0 = \sum_{\text{loops}} K^b N^l, \quad (63)$$

with  $b$  and  $l$  denoting the total number of occupied bonds and separate loops forming a given tangle. In Eq. (63), the loops are no longer considered to be rooted, i.e., they can start and end at any spacetime coordinate

in the system. In comparison with rooted closed paths, i.e., closed paths all starting at a given spacetime coordinate, this yields a spacetime volume factor  $\Omega$ . In the continuum, Eq. (63) translates into the path integral representation

$$Z_0 = \sum_{l=0}^{\infty} \frac{1}{l!} \left( \frac{N}{2} \right)^l \prod_{r=1}^l \left[ \Omega \int_0^{\infty} \frac{ds_r}{s_r} \oint Dx_r(s'_r) \right] e^{-W_0^{(l)}}, \quad (64)$$

as follows from Eq. (60). Here,  $W_0^{(l)}$  denotes the extension of the single particle action (33) to  $l$  particles:

$$W_0^{(l)} = \sum_{r=1}^l \int_0^{s_r} ds'_r \left[ \frac{1}{4} \dot{x}_r^2(s'_r) + m^2 \right]. \quad (65)$$

### 2.3. $|\phi|^4$ Field Theory

We next perturbatively include the interaction in the theory (2). At the level of the partition function (1), this boils down to expanding the interaction term of the action in a Taylor series

$$e^{-(g/4!)a^d \sum_x \varphi_x^4} = 1 - \frac{g}{4!} a^d \sum_x \varphi_x^4 + \frac{1}{2!} \left( \frac{g}{4!} \right)^2 a^{2d} \sum_{x,x'} \varphi_x^4 \varphi_{x'}^4 + \dots \quad (66)$$

The terms in this expansion can all be represented by Feynman diagrams.<sup>10,12</sup> Figure 3 shows the 2- and 3-loop diagrams contributing to  $\ln Z$  as an example. Each loop, which are considered to have no orientation, carries a factor of  $N$ . The contact interaction is represented by a dashed line for convenience, each carrying a weight  $\propto g$ . In the equivalent spacetime approach, Feynman diagrams are understood as spacetime diagrams. Each loop of a Feynman diagram is expressed in a hopping expansion as in the noninteracting theory, with the interaction standing for an intersection between different worldlines or between different parts of a single worldline (self-intersection). In addition to the ones indicated, a worldline contributing to a given Feynman diagram may have further intersections, but these are treated as in the noninteracting case, i.e., as nonexistent. Put differently, apart from the intersections explicitly indicated, the particle trajectories still behave as phantom paths.

Picturing the topology of closed worldlines, the first Feynman diagram ( $\propto N$ ) of the 2-loop contributions ( $\propto g^2$ ) in Fig. 3 represents single closed particle trajectories of arbitrary length and shape with one self-intersection carrying a factor of  $g$ . The second Feynman diagram ( $\propto N^2$ ) represents two



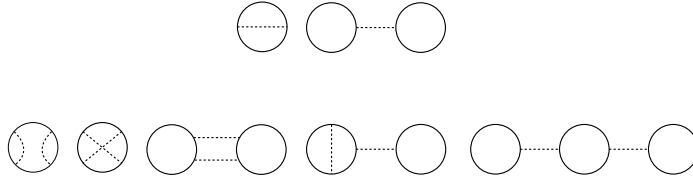


Fig. 3. Two- and 3-loop Feynman diagrams contributing to  $\ln Z$  of the  $|\varphi|^4$  theory.

intersecting closed worldlines. The 3-loop contributions ( $\propto g^3$ ) represent single closed worldlines with two self-intersections (1st and 2nd diagram  $\propto N$ ), two closed worldlines intersecting twice (3rd diagram  $\propto N^2$ ), two closed worldlines intersecting once with one of the two having in addition one self-intersection (4th diagram  $\propto N^2$ ), and finally three closed worldlines (last diagram  $\propto N^3$ ) connected by two intersections.

Similarly, the  $n$ th order contributions to  $\ln Z$ , corresponding to the  $(n-1)$ th term ( $\propto g^{n-1}$ ) in the Taylor expansion (66), all involve a total of  $n-1$  intersections (including self-intersections) and up to  $n$  separate loops. The resulting loop gas is similar to that of the free theory, but the random loops are no longer phantom loops as the intersections explicitly indicated carry a weight  $\propto g$ . In the path integral formulation, this is reflected by an additional steric repulsion in the worldline action,

$$W^{(l)} = \sum_{r=1}^l \int_0^{s_r} ds'_r \left[ \frac{1}{4} \dot{x}_r^2(s'_r) + m^2 \right] + \frac{g}{6} \sum_{r,r'=1}^l \int_0^{s_r} ds'_r \int_0^{s_{r'}} ds'_{r'} \delta[x_r(s'_r) - x_{r'}(s'_{r'})], \quad (67)$$

where the sums  $\sum_r$  and  $\sum_{r'}$  extend over the  $l$  particle trajectories assumed to be present. The net result is that (self-)intersections are suppressed and the random loops tend to become mutually and self-avoiding the more so, the larger the coupling constant  $g$  becomes. Turning on the interaction thus changes the typical form of the random loops and in particular their fractal structure.

To derive Eq. (67), we follow Symanzik<sup>36</sup> and write the interaction term in the action (2) in the continuum limit as a functional integral over an auxiliary field  $\sigma$

$$\exp \left( -\frac{g}{4!} \int d^d x \varphi^4 \right) = \int D\sigma \exp \left[ -\int d^d x \left( \frac{6}{g} \sigma^2 - i\sigma \varphi^2 \right) \right], \quad (68)$$

up to an irrelevant prefactor. The partition function (1) then becomes in the continuum limit

$$\begin{aligned}
Z &= \int D\varphi D\sigma \exp \left\{ - \int d^d x \left[ \frac{1}{2} (\partial_\mu \varphi)^2 + \frac{m^2}{2} \varphi^2 - i\sigma \varphi^2 + \frac{6}{g} \sigma^2 \right] \right\} \\
&= \int D\sigma \text{Det}^{-N/2} (-\partial_\mu^2 + m^2 - 2i\sigma) \exp \left( -\frac{6}{g} \int d^d x \sigma^2 \right) \\
&= \int D\sigma \sum_{l=0}^{\infty} \frac{1}{l!} \left( \frac{N}{2} \right)^l \prod_{r=1}^l \left[ \Omega \int_0^\infty \frac{ds_r}{s_r} \oint Dx_r(s'_r) \right] \exp \left( -\frac{6}{g} \int d^d x \sigma^2 \right) \\
&\quad \times \exp \left( - \sum_{r=1}^l \int_0^{s_r} ds'_r \left\{ \frac{1}{4} \dot{x}_r^2(s'_r) + m^2 - 2i\sigma[x_r(s'_r)] \right\} \right) \quad (69)
\end{aligned}$$

where the last equality follows from the previous result (64). The auxiliary field  $\sigma$  is a function of the coordinates along the particle trajectories,  $\sigma = \sigma[x_r(s'_r)]$ . A simple Gaussian integration yields

$$\begin{aligned}
&\int D\sigma \exp \left\{ -\frac{6}{g} \int d^d x \sigma^2 + 2i \sum_{r=1}^l \int_0^{s_r} ds'_r \sigma[x_r(s'_r)] \right\} \\
&= \exp \left\{ -\frac{g}{6} \sum_{r,r'=1}^l \int_0^{s_r} ds'_r \int_0^{s_{r'}} ds'_{r'} \delta[x(s'_r) - x(s'_{r'})] \right\}, \quad (70)
\end{aligned}$$

again up to an irrelevant prefactor. Using this in the last expression for  $Z$ , we obtain the spacetime representation of the partition function of the  $\varphi^4$  theory

$$Z = \sum_{l=0}^{\infty} \frac{1}{l!} \left( \frac{N}{2} \right)^l \prod_{r=1}^l \left[ \Omega \int_0^\infty \frac{ds_r}{s_r} \oint Dx_r(s'_r) \right] e^{-W^{(l)}}, \quad (71)$$

with the classical action  $W^{(l)}$  of the point particles tracing out their world-lines given in Eq. (67). The  $l$ th term in this sum describes a tangle of  $l$  loops. Since the number of loops can be arbitrary large, Eq. (71) denotes the partition function of a grand canonical ensemble of fluctuation loops, each of arbitrary length and shape, with steric repulsion.

Surprisingly, as was first pointed out by Balian and Toulouse,<sup>37</sup> the noninteracting theory can be recovered from the interacting theory by taking the number of field components  $N \rightarrow -2$ . Consider a contribution to the partition function involving the first vertex in Fig. 4. Assume that leg 1 is connected through the rest of the Feynman diagram to leg 2. Both

legs carry the same spin index  $\alpha$ , which after taking the sum yields a factor of  $N$ . Legs 3 and 4 are necessarily also connected through the rest of the Feynman diagram. They carry the same spin index  $\beta$ , say, which after taking the sum also yields a factor of  $N$ . Replacing the first vertex with the second or third vertex in Fig. 4 yields identical contributions save for a change in topology regarding the routings of the spin indices. Specifically, the graph with the first vertex involves two different sets of spin indices:  $\alpha$  and  $\beta$ , whereas the graphs with the second or third vertex involve only a single set of spin indices as  $\alpha = \beta$ . Since the first graph carries an extra factor of  $N = -2$  (the loop fugacity) after the sum over the spin index is taken, the three graphs cancel. All other graphs involving vertices cancel in the same fashion three by three. What remains are phantom loops of a noninteracting theory.

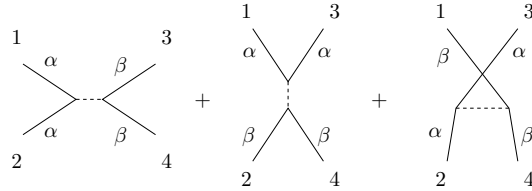


Fig. 4. The representation of the vertex of the  $\varphi^4$  theory by a dashed line makes the routings of the field components, labeled by  $\alpha$  and  $\beta$ , explicit.

## 2.4. $O(N)$ Spin Model

Whereas the free theory discussed in Sec. 2.1 corresponds to taking the coupling constant  $\lambda \rightarrow 0$  in the action (8), the  $O(N)$  spin model corresponds to taking the opposite limit,  $\lambda \rightarrow \infty$ . As for  $\lambda \rightarrow 0$ , the theory becomes quadratic also in this limit of infinite repulsion. The theory is nevertheless nontrivial because of the fixed-length constraint  $\phi_n^2 = N$  at each lattice site. Instead of considering the conventional Boltzmann weight  $\exp(K\phi_n \cdot \phi_{n'})$ , often a simplified representative of the  $O(N)$  universality class is studied, obtained by truncating that weight<sup>38</sup>

$$Z = \text{Tr} \prod_{\langle n, n' \rangle} (1 + K\phi_n \cdot \phi_{n'}). \quad (72)$$

The product is restricted to nearest neighbor pairs. The remaining factor in the on-site measure (10) becomes trivial in this limit and has been ignored.

The main difference with the original spin model is that in the truncated model bonds cannot be multiply occupied. It is generally accepted that this simplification does not change the universal properties of the theory.

The hopping expansion is usually referred to the *high-temperature expansion* in the context of spin models. Also for the truncated model, it corresponds to expanding the partition function in terms of the parameter  $K$ . The contributions to  $Z$  can again be visualized by graphs on the lattice.<sup>13</sup> As will be detailed below for the Ising model, only closed graphs with an even number of occupied bonds connecting each vertex yield nonzero contributions. The virtue of the truncated model is that bonds cannot be multiply occupied. In contrast, no restriction on multiple occupancies exists in the representation with the usual Boltzmann weight. When formulated on a two-dimensional honeycomb lattice, which has coordination number  $z = 3$ , the high-temperature graphs of the truncated model are automatically mutually and self-avoiding:<sup>38</sup> a given lattice site is either empty or has one bond entering and one leaving the site (see Fig. 5).

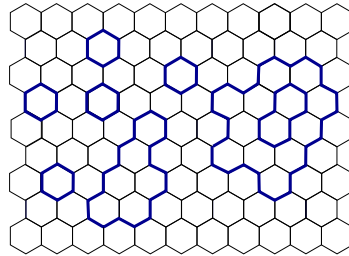


Fig. 5. Closed high-temperature graphs on a honeycomb lattice automatically form mutually and self-avoiding loops.

The partition function can then be written geometrically as a sum over all possible mutually and self-avoiding (MSA) loops,<sup>38</sup>

$$Z = \sum_{\substack{\text{MSA} \\ \text{loops}}} N^l K^b, \quad (73)$$

with  $b$  and  $l$  the number of occupied bonds and separate loops forming the graph. Equation (73) constitutes the high-temperature representation of the partition function. As for the noninteracting field theory (63), each occupied bond carries a weight  $K$  (bond fugacity) and each loop carries a weight  $N$  (loop fugacity). Whereas the random loops of the noninteracting

field theory are phantom loops that can freely intersect and share bonds, here they are mutually and self-avoiding. As before, they physically denote the worldlines of the particles described by the quantum field theory.

The  $O(N)$  spin-spin correlation function

$$\langle \phi_n^\alpha \phi_{n'}^\beta \rangle = \frac{1}{Z} \prod_m \int d\phi_m \phi_n^\alpha \phi_{n'}^\beta \exp \left( K \sum_{\langle m, m' \rangle} \phi_m \cdot \phi_{m'} \right), \quad (74)$$

is represented diagrammatically by a modified partition function, obtained by requiring that the two sites  $n$  and  $n'$  are connected by an open high-temperature graph.<sup>13</sup> On a honeycomb lattice, the scaling part of the correlation function is given by the connected graphs

$$\langle \phi_n^\alpha \phi_{n'}^\beta \rangle \sim \frac{1}{2} \delta_{\alpha, \beta} \sum_{\text{graphs}} K^b = \frac{1}{2} \delta_{\alpha, \beta} \sum_b z_b(n, n') K^b, \quad (75)$$

where  $z_b(n, n')$  is the number of (open) mutually and self-avoiding graphs along  $b$  bonds connecting the lattice sites  $n$  and  $n'$ . Strictly speaking,  $\langle \phi_n^\alpha \phi_{n'}^\beta \rangle < \frac{1}{2} \delta_{\alpha, \beta} \sum_{\text{graphs}} K^b$  as the cancellation of the disconnected graphs in the numerator and  $Z$  in the denominator, required for an equality, is not complete: For a given open graph, certain loops present in  $Z$  are forbidden in the modified partition function as they would intersect the open graph, or occupy bonds belonging to it, which is not allowed. In other words, the presence of an open graph influences the loop gas and *vice versa*. Since each loop carries a factor  $N$ , the loop gas is absent in the limit  $N \rightarrow 0$ , pioneered by de Gennes.<sup>14</sup> The inequality in Eq. (75) becomes an equality in this limit, and the open graphs become ordinary self-avoiding random walks on a honeycomb lattice. These walks physically describe polymers in good solvents at sufficiently high temperatures so that the van der Waals attraction between monomers is irrelevant. For the noninteracting theory, where the worldlines are phantom trajectories, the loops cancel, so that the corresponding correlation function is exactly given by the open trajectories connecting the endpoints [see Eq. (16)].

For a  $d$ -dimensional hypercubic lattice, the coordination number is  $z = 2d$ , so that intersections are now possible. Although the bonds of the truncated model (72) can by construction still not be multiply occupied, the high-temperature graphs are no longer mutually and self-avoiding. After rescaling the bond fugacity  $K \rightarrow K/N$ , the partition function (72) can

be written as<sup>39</sup>

$$Z = \sum_{\text{loops}} \nu_2^{m_2} \nu_4^{m_4} \cdots \nu_{2d}^{m_{2d}} N^l \left( \frac{K}{N} \right)^b, \quad (76)$$

where  $m_2, \dots, m_{2d}$  indicate the number of intersections of  $2k$  bonds ( $k = 1, \dots, d$ ) forming a given tangle of  $b$  bonds and  $l$  loops. An intersection of  $2k$  bonds carries the weight<sup>40</sup>

$$\nu_{2k} = \frac{N^k \Gamma(N/2)}{2^k \Gamma(k + N/2)} = \frac{N^k}{N(N+2) \cdots (N+2k-2)}. \quad (77)$$

Due to the rescaling of the bond fugacity,  $\nu_2 = 1$  for all  $N$ . In the limit  $N \rightarrow 0$ , only the weight  $\nu_2$  survives as  $\nu_{2k} \rightarrow 0$  for  $k > 1$ , implying that even on a hypercubic lattice, intersections are completely suppressed and the high-temperature graphs reduce to self-avoiding walks.

In the opposite limit,  $N \rightarrow \infty$ , all the vertex weights become unity  $\nu_{2k} \rightarrow 1$ , and the partition function (76) takes the noninteracting form (63) after undoing the rescaling of the bond fugacity. The only difference with the noninteracting theory is that for a given number of set bonds  $b$ , only the graph with the highest number of loops needs to be included as it dominates all other graphs. This limit corresponds to the so-called spherical model.<sup>13</sup>

The loop representation (76), featuring colorless loops, obtains by resolving a vertex where  $2k$  bonds of an high-temperature graph meet into all possible routings of the paths (see Figs. 6 and 7). The number of rout-

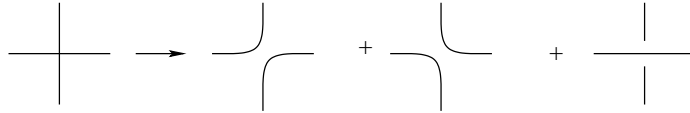


Fig. 6. A vertex with four bonds ( $k = 2$ ) resolved into three possible routings of the paths.

ings equals the number of ways  $2k$  objects can be divided into  $k$  distinct pairs, i.e.,  $(2k-1)!!$ . Each of the routings carries the same weight. A given high-temperature graph is thus resolved into loop configurations, and the partition function (76) describes a loop gas, as does Eq. (73). The loops physically represent worldlines that can now intersect. Although loops on a honeycomb lattice cannot do so, for both the honeycomb and square lattice the same large-scale behavior is obtained. This implies that the operator

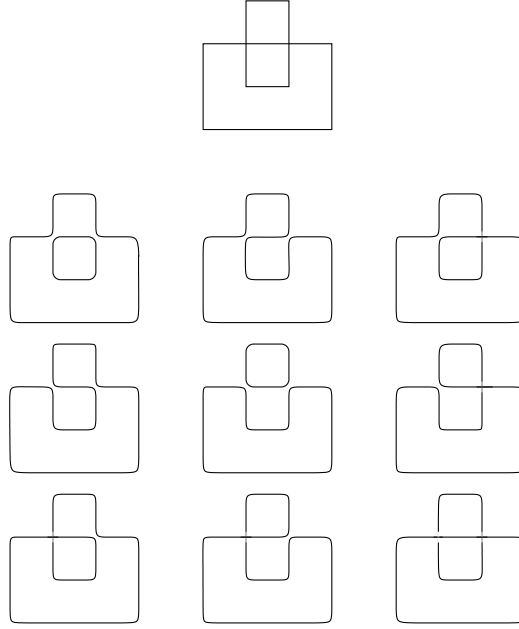


Fig. 7. A graph (top panel) involving two vertices with four bonds ( $k = 2$ ) is resolved into 9 different loop configurations according to the rule displayed in Fig. 6.

which introduces intersections is an irrelevant perturbation at the critical point.<sup>41</sup>

It is worth pointing out that in the high-temperature representation, the observation that  $N = -2$  describes phantom loops is far from obvious. On a square lattice, for example, a graph of  $b$  bonds and one vertex where four bonds meet contributes the following term to the partition function,

$$\lim_{N \rightarrow -2} \nu_4 N(N+2) \left( \frac{K}{N} \right)^b = (-2)^2 \left( -\frac{K}{2} \right)^b, \quad (78)$$

which is finite because the weight factor  $\nu_4$  given in Eq. (77) diverges in the limit  $N \rightarrow -2$ . The diagrams no longer cancel three by three as they did in Sec. 2.3

## 2.5. Ising Model

As an explicit example, we consider the simplest  $O(N)$  model, viz. the Ising model ( $N = 1$ ) on a square lattice. The model is defined by the Hamiltonian

$$H = -J \sum_{\langle nn' \rangle} \phi_n \phi_{n'}, \quad (79)$$

where the spins can take only two values  $\phi_n = \pm 1$ , and the interaction parameter  $J$  is taken to be unity. The standard partition function reads

$$Z = \text{Tr} e^{-\beta H} = \text{Tr} \prod_{\langle nn' \rangle} e^{\beta \phi_n \phi_{n'}}, \quad (80)$$

with the trace  $\text{Tr}$  denoting the sum over all possible spin configurations. In the context of statistical physics,  $\beta$  denotes the inverse temperature  $\beta = 1/k_B T$ , with  $k_B$  Boltzmann's constant. In the present context, we regard  $\beta$  as coupling constant. Because of the identity

$$e^{\beta \phi_n \phi_{n'}} = \cosh \beta (1 + K \phi_n \phi_{n'}), \quad (81)$$

with  $K = \tanh \beta$ , the standard representation can be rewritten in the truncated form (72) as:

$$Z = (\cosh \beta)^{2N} \text{Tr} \prod_{\langle nn' \rangle} (1 + K \phi_n \phi_{n'}) \quad (82)$$

up to an irrelevant prefactor. Here,  $2N$  denotes the total number of bonds on a square lattice with  $N$  sites and periodic boundary conditions. The right hand contains a total of  $2N$  factors, one for each bond, and therefore a total of  $2^{2N}$  terms when multiplied out. Each term can be visualized by a graph along the bonds on the lattice, with each bond representing a pair of adjacent spins. Because of the trace in the definition of the partition function, a graph having a loose end does not contribute to  $Z$ . Indeed, let the spin at the loose end be  $\phi_n$  then the sum over its possible configurations yields zero,  $\sum_{\phi_n=\pm 1} \phi_n = 0$ . As a result, only *closed* graphs contribute. Similarly, only those closed graphs with an even number of bonds, i.e., two or four for a square lattice, connecting each vertex of the graph yield nonzero contributions. Such a vertex contributes a factor of two as  $\sum_{\phi_n=\pm 1} \phi_n^m = 2$  for  $m$  even. The high-temperature representation of the Ising model therefore involves a sum over all possible closed graphs that can be drawn on the lattice:

$$Z = (\cosh \beta)^{2N} 2^N \sum_{\substack{\text{closed} \\ \text{graphs}}} K^b. \quad (83)$$



A graph of  $b$  bonds can be build from various disconnected closed sub-graphs. The high-temperature representation is to be compared with the loop representation (76), which reduces to

$$Z = \sum_{\text{loops}} \left(\frac{1}{3}\right)^m K^b, \quad (84)$$

for  $N = 1$  on a square lattice, with  $m$  denoting the number of vertices with four bonds. Remembering that the loop representation is obtained by resolving each of these vertices according to the rule given in Fig. 6, we see that apart from an irrelevant prefactor the two expressions coincide. The Ising model ( $N = 1$ ) is special as the loop fugacity is unity, so that the contribution of a closed graph depends only on the number of bonds it occupies.

The correlation function of the Ising model,

$$\begin{aligned} \langle \phi_n \phi_{n'} \rangle &= \frac{1}{Z} \text{Tr} \phi_n \phi_{n'} \prod_{\langle mm' \rangle} e^{\beta \phi_m \phi_{m'}}, \\ &= \frac{1}{Z} (\cosh \beta)^{2N} \text{Tr} \phi_n \phi_{n'} \prod_{\langle mm' \rangle} (1 + K \phi_m \phi_{m'}). \end{aligned} \quad (85)$$

can similarly be visualized by graphs on the lattice. Each graph now contains a subgraph connecting the lattice sites  $n$  and  $n'$ . All other subgraphs must be closed and, except for the endpoints, all vertices must be even as before. In terms of these graphs,

$$\langle \phi_n \phi_{n'} \rangle = \frac{1}{Z} (\cosh \beta)^{2N} 2^N \sum_{\text{graphs}} K^b. \quad (86)$$

## 2.6. Summary

In the spacetime approach to quantum field theory on a lattice, which is geometric in nature, the partition function and the correlation function are calculated in a hopping expansion, thus reducing the problem to counting paths on the lattice. Physically, the paths represent the worldlines traced out by the particles when hopping from one lattice site, representing a spacetime cell, to an adjacent site. The noninteracting lattice field theory features phantom worldlines that can freely intersect and share bonds. When the self-interaction is turned on, by taking the coupling constant  $\lambda > 0$ , intersections carry an energy penalty. This has the effect to suppress such configurations and as a result the particle trajectories tend to avoid

themselves. In the limit of infinite repulsion  $\lambda \rightarrow \infty$ , the  $\phi^4$  lattice field theory reduces to the  $O(N)$  spin model. The hopping expansion, known in this context as the high-temperature expansion, takes a particular simple form when the truncated  $O(N)$  model (72) is implemented on a honeycomb lattice. The worldlines are then by construction mutually and self-avoiding. Since the large-scale behavior of this representative of the  $O(N)$  universality class on the honeycomb lattice is the same as for the generic  $\phi^4$  field theory defined on a square lattice, both multiply occupancy of bonds and intersections are irrelevant. At large scales, both loop gases have the same fractal structure. Even when considering weak repulsion by taking  $\lambda$  small, after coarse-graining the fractal structure of the loops appears the same as in the limit  $\lambda \rightarrow \infty$ . This limit therefore governs the large-scale behavior.

### 3. Critical Properties

In this section, the critical properties of the  $O(N)$  universality class are discussed from the perspective of worldlines. In particular, the fractal structure of the loop gas featuring in the spacetime approach to fluctuating fields close to the critical point is studied. It is shown how the critical exponents characterizing the phase transition can be obtained from the fractal structure of these geometrical objects. The discussion is geared after percolation theory, which is purely geometric in nature.<sup>42</sup>

#### 3.1. Fractal Structure

Consider the  $O(N)$  theory close to the point where it undergoes a continuous phase transition to the ferromagnetic state, where the spins prefer to point in one direction in spin space. This phase transition is associated with the spontaneous breaking of the  $O(N)$  symmetry to the subgroup  $O(N-1)$  which includes rotations about the preferred spin direction. The logarithm of the partition function of the interacting theory can in the vicinity of this critical point be written in a form similar to the one found in Eq. (54) for the noninteracting theory as

$$\ln Z \sim \sum_b \ell_b. \quad (87)$$

The worldline loop distribution  $\ell_b$  asymptotically splits into two factors as it did for the phantom loops in Eq. (55):

$$\ell_b \sim b^{-\tau} e^{-\theta b}, \quad (88)$$

with  $\tau$  an exponent characterizing the interacting theory. The value  $\tau = d/2 + 1$  found for phantom loops is typical for a noninteracting theory where the loops are simple closed Brownian trajectories. Formally, Eq. (87) is the same as for clusters in percolation theory close to the percolation threshold. As in that context,<sup>42</sup>  $\tau$  can be related to the fractal dimension of the loops. Consider the square radius of gyration  $R_b^2$  of a loop of  $b$  steps

$$R_b^2 = \frac{1}{b} \sum_{i=1}^b (n_i - \bar{n})^2 = \frac{1}{2b^2} \sum_{i,j=1}^b (n_i - n_j)^2, \quad (89)$$

with  $n_i$  denoting the lattice sites visited by the particle while tracing out its worldline on the spacetime lattice, and  $\bar{n} = (1/b) \sum_{i=1}^b n_i$  the center of mass of the loop. Asymptotically, the average  $\langle R_b^2 \rangle$  scales with the number of steps  $b$  taken as

$$\langle R_b^2 \rangle \sim b^{2/D}, \quad (90)$$

which defines the Hausdorff, or fractal dimension  $D$ . This average yields the typical linear size of a loop of  $b$  steps. Specifically, such a loop is distributed over a volume of typical linear size  $\langle R_b^2 \rangle^{1/2}$ . Given the definition of the loop distribution  $\ell_b$  as the average number (per lattice site) of loops of  $b$  steps present, it follows that  $b\ell_b$  is the probability that a randomly chosen lattice site belongs to such a loop, and

$$b\ell_b \sim 1 / \langle R_b^2 \rangle^{d/2}, \quad (91)$$

with  $d$  the dimension of the spacetime box. This leads to the relation

$$\tau = \frac{d}{D} + 1, \quad (92)$$

which is formally the same as in percolation theory.<sup>42</sup>

### 3.2. Loop Proliferation

The Boltzmann factor in the loop distribution (88) exponentially suppresses long loops as long as the line tension  $\theta$  is finite. Upon approaching the critical point, the line tension vanishes as a power law,

$$\theta \sim (K_c - K)^{1/\sigma}, \quad (93)$$

with  $\sigma$  a second exponent characterizing the loop distribution. When this happens, the loops can grow arbitrarily long at no cost and the entire system becomes<sup>43</sup> “pierced through and through with” worldlines. It is through this *loop proliferation*<sup>20</sup> that a phase transition manifests itself in

the spacetime approach. The phenomenon is completely analogous to the sudden appearance at the percolation threshold of a cluster spanning the infinite lattice in percolation phenomena.

In the field theoretic approach, the phase transition manifests itself through a nonzero vacuum expectation value of the field  $\phi_n^\alpha$ , where the component  $\alpha$  indicates the preferred spin direction spontaneously chosen by the system. Since all possible directions are equivalent, the system can choose any of these. On a finite lattice, the system can easily change its preferred direction. This is in particular the case for Monte Carlo simulations using a nonlocal update, such as the Swendsen-Wang,<sup>44</sup> or Wolff<sup>45</sup> algorithm, in which not individual spins are updated, but entire clusters. For this reason, the following order parameter is frequently used in lattice simulations:<sup>46</sup>

$$\mathcal{O} = \frac{1}{L^d} \left[ \sum_{\alpha} \left( \sum_n \phi_n^\alpha \right)^2 \right]^{1/2}. \quad (94)$$

With this choice of the order parameter, all possible directions are treated equally. In the normal phase, the expectation value of this operator vanishes. At the critical point, a condensate forms and a nonzero expectation value develops,

$$\langle \mathcal{O} \rangle \neq 0, \quad (95)$$

typical for the ferromagnetic state with the spins pointing in a preferred direction in spin space. Those particles tracing out long worldlines all belong to the condensate.

The loop distribution (88) is related to the number of paths  $z_b(a)$  of  $b$  steps returning to a site adjacent to the initial position through

$$\ell_b = \frac{1}{b} z_b(a) K^b. \quad (96)$$

Because  $z_b(a)$  refers to closed worldlines, the factor  $1/b$  is included to prevent overcounting as a given loop can be traced out starting at any lattice site along that loop. It should be noted that in Eq. (96) rooted loops are considered, i.e., all loops run through an arbitrary but fixed lattice site  $n$ . The relation (96) implies that  $z_b(a)$  scales as

$$z_b(a) K^b \sim b^{-d/D} e^{-\theta b}. \quad (97)$$

Similarly, the number of paths  $z_b$  of  $b$  steps starting at  $n$  and ending at an arbitrary lattice site defined in Eq. (40) scales as

$$z_b K^b \sim b^{\vartheta/D} e^{-\theta b}, \quad (98)$$

with  $\vartheta$  a new exponent, characterizing the number of ways an open path of  $b$  steps can be embedded in the lattice. It is worth pointing out that in contrast to the loop exponents  $\tau$  and  $\sigma$ , this third exponent refers to open paths. Its value is expected to be positive because the number of possible rooted open paths with no constraint on their endpoints increases with the number of steps  $b$ . This is in contrast to the loop distribution (88), where the algebraic factor decreases with increasing  $b$ , reflecting the increasing difficulty for a path to close. According to Eq. (39), the ratio of  $z_b(n, n')$  and  $z_b$  defines the probability  $P_b(n, n')$  for a particle to move from the lattice site  $n$  on the spacetime lattice to  $n'$  in  $b$  steps. On general grounds, it scales at criticality as:

$$P_b(n, n') \sim b^{-d/D} \mathbf{P}\left(|n - n'|/b^{1/D}\right), \quad (99)$$

with  $\mathbf{P}$  a scaling function. This generalizes the Gaussian distribution (44) found for the noninteracting theory. Consistency of the three scaling formulas (97), (98), and (99), requires, as was first shown by McKenzie and Moore<sup>47</sup> for self-avoiding random walks, that the scaling function  $\mathbf{P}(t)$  must vanish for  $t \rightarrow 0$  as a power law,

$$\mathbf{P}(t) \approx t^\vartheta, \quad (100)$$

with the same exponent governing the *asymptotic* behavior (98) of the number  $z_b$  of open paths at the critical point ( $\theta = 0$ ).

### 3.3. Critical Exponents

As in percolation theory, the loop exponent  $\sigma$  is related to the exponent  $\nu$ , which specifies how the correlation length  $\xi$  diverges at the critical point,

$$\xi \sim |K - K_c|^{-\nu}. \quad (101)$$

Physically,  $\xi$  indicates the typical length scale in the system. The radius of gyration—a second typical length scale—can be written in terms of  $\xi$  as

$$\langle R_b \rangle = \xi \mathbf{R}(b\theta), \quad (102)$$

where  $\mathbf{R}$  is a scaling function and  $\theta$  is the same parameter as in the loop distribution (88). From the asymptotic behavior (90), the divergence of the correlation length, and the vanishing (93) of the line tension  $\theta$  as  $K_c$  is approached, the relation<sup>31</sup>

$$\nu = \frac{1}{\sigma D}, \quad (103)$$

or

$$\nu = \frac{\tau - 1}{d\sigma}, \quad (104)$$

follows. These relations are formally identical to those in percolation theory.

The rest of the thermal critical exponents can equally well be expressed in terms of the loop exponents and  $\vartheta$ . To derive these expressions, we write the correlation function in terms of  $z_b(n, n')$  as on the honeycomb lattice [see Eq. (75)]

$$\langle \phi_n^\alpha \phi_{n'}^\beta \rangle \sim \frac{1}{2} \delta_{\alpha, \beta} \sum_b z_b(n, n') K^b = \frac{1}{2} \delta_{\alpha, \beta} \sum_b z_b P_b(n, n') K^b. \quad (105)$$

When evaluated at criticality, where

$$\langle \phi_n^\alpha \phi_{n'}^\beta \rangle \sim \delta_{\alpha, \beta} / |n - n'|^{d-2+\eta}, \quad (106)$$

Eq. (105) gives

$$\eta = 2 - D - \vartheta. \quad (107)$$

This relation, with  $\vartheta$  defined by Eq. (100), was recently proposed for the three-dimensional XY, i.e., O(2) model in Ref. [48]. This model describes the superfluid phase transition in  $^4\text{He}$ .

Finally, using the definition of the magnetic susceptibility  $\chi$ ,

$$\chi = \sum_{n'} \langle \phi_n \cdot \phi_{n'} \rangle \sim \sum_b z_b K^b, \quad (108)$$

which diverges as  $\chi \sim |K - K_c|^{-\gamma}$ , we find

$$\gamma = \frac{1}{\sigma} \left( 1 + \frac{\vartheta}{D} \right). \quad (109)$$

The explicit expressions given for  $\nu$ ,  $\eta$ , and  $\gamma$  satisfy Fisher's scaling relation,  $\gamma/\nu = 2 - \eta$ , and

$$\frac{\gamma}{\nu} = D + \vartheta. \quad (110)$$

With  $\nu = (\tau - 1)/d\sigma$ , Eq. (54) yields the scaling relation  $d\nu = 2 - \alpha$ , where  $\alpha$  determines the scaling behavior of the free energy close to the critical point,

$$\ln Z \sim |K - K_c|^{2-\alpha}. \quad (111)$$

The expressions for the other exponents follow by using the remaining scaling relations. We thus have shown that all the thermal critical exponents are

determined by the configurational entropy exponents for closed and open particle trajectories,  $\tau$  and  $\vartheta$ , respectively, and by  $\sigma$ .

It is worth noting that the thermal critical exponents depend on only *two* independent variables, viz.  $D + \vartheta$  and  $\sigma D$ . Their significance in field theory is that they determine the anomalous scaling dimensions of the  $\varphi$  and  $\varphi^2$  fields

$$d_\varphi = \frac{1}{2}(d - D - \vartheta), \quad d_{\varphi^2} = d - \sigma D, \quad (112)$$

respectively.

### 3.4. Self-Avoiding Random Walks

Before applying the results of the previous section to the two-dimensional  $O(N)$  spin model with arbitrary  $-2 \leq N \leq 2$ , let us first verify that these general results are consistent with the results known in the polymer limit  $N \rightarrow 0$ ,<sup>14</sup> where, as we saw below Eq. (77), the high-temperature graphs reduce to self-avoiding walks. Through the exact enumeration and analysis of the number of self-avoiding loops on a square lattice up to length 110, the value  $\tau = 5/2$  for the loop exponent  $\tau$  has been established to very high precision.<sup>49</sup> According to Eq. (92), this corresponds to the fractal dimension  $D = 4/3$ —a value that has been independently established to high precision in that same study by determining the average square radius of gyration  $\langle R_b^2 \rangle$  of the loops. In a related study,<sup>50</sup> where the number  $z_b$  of self-avoiding walks on a square lattice up to length 71 has been enumerated and analyzed, the value of the exponent  $\vartheta$ , characterizing the open trajectories has been established. Specifically, the value  $\vartheta/D = 11/32$  was found to high precision, yielding  $\vartheta = 11/24$ .

In most studies on self-avoiding walks, the fractal dimension of the walks is simply equated to the inverse correlation length. As follows from Eq. (103), this corresponds to setting  $\sigma = 1$ . A closer inspection of de Gennes' original work on the  $N \rightarrow 0$  limit reveals that there indeed  $\sigma = 1$ .

To sum up, the two configurational entropy exponents  $\tau$  (loops) and  $\vartheta$  (open paths), and  $\sigma$  for a self-avoiding walk in two dimensions are given by

$$\tau = 5/2, \quad \vartheta = 11/24, \quad \sigma = 1. \quad (113)$$

With these values, all the critical exponents of the two-dimensional  $O(N \rightarrow 0)$  model can be found through the relations of the previous subsection and standard scaling relations.

### 3.5. $O(N)$ Models

The class of two-dimensional  $O(N)$  models for  $-2 \leq N \leq 2$  can be parametrized as

$$N = -2 \cos\left(\frac{\pi}{\bar{\kappa}}\right), \quad (114)$$

with  $\frac{1}{2} \leq \bar{\kappa} \leq 1$ . The fractal dimension  $D$  of the high-temperature loops is known exactly<sup>51</sup>

$$D = 1 + \frac{\bar{\kappa}}{2}, \quad (115)$$

leading to  $\tau = (6 + \bar{\kappa})/(2 + \bar{\kappa})$ . The observable whose scaling dimension is given by this fractal dimension consists of two spins in different spin states placed at the same site:  $\phi_n^\alpha \phi_n^\beta$ , with  $\alpha \neq \beta$ .<sup>38</sup> It physically measures the tendency of spins to align, as becomes intuitively clear by remembering that the spins connected by a high-temperature graph are all in the same spin state.

While the fractal dimension of the high-temperature loops is known exactly in two dimensions, the value of the entropy exponent  $\vartheta$  for open paths has to our knowledge not been directly established for  $N \neq 0$ . In two dimensions, it can be established indirectly<sup>32</sup> by considering the Potts model—a closely related spin model.

That model was reformulated by Fortuin and Kasteleyn<sup>52</sup> in a purely geometric fashion in terms of suitably defined spin clusters. The thermal phase transition is marked by a proliferation of these clusters, which moreover have the thermal critical exponents encoded in their fractal structure. Percolation observables such as the average cluster size and the percolation strength, defined as the probability that a randomly chosen site belongs to the percolating cluster, serve as improved estimators for the magnetic susceptibility and the magnetization, respectively. In other words, the thermal critical exponents of the Potts model can be determined by studying the fractal structure of these so-called Fortuin-Kasteleyn clusters, with the exponents defined as in percolation theory. In two dimensions, the fractal dimension  $D_C$  of the Fortuin-Kasteleyn clusters is known exactly<sup>53</sup>

$$D_C = 1 + \frac{\bar{\kappa}}{2} + \frac{3}{8} \frac{1}{\bar{\kappa}}, \quad (116)$$

where the  $Q$ -state Potts models are parametrized in terms of the same parameter  $\bar{\kappa}$  parametrizing the  $O(N)$  models as

$$\sqrt{Q} = -2 \cos(\pi \bar{\kappa}), \quad (117)$$



with  $\frac{1}{2} \leq \bar{\kappa} \leq 1$ , so that  $0 \leq Q \leq 4$ . The  $Q \rightarrow 0$  Potts model ( $\bar{\kappa} = \frac{1}{2}$ ) describes standard percolation theory. Surprisingly, the external perimeters of the Fortuin-Kasteleyn clusters have the same fractal dimension  $D$  as the  $O(N)$  loops.<sup>54</sup> For example, the external perimeters of clusters in standard percolation theory have the dimension  $\frac{4}{3}$  as have self-avoiding random walks ( $\bar{\kappa} = \frac{2}{3}$ ). It can be shown that the entropy exponent  $\vartheta$  for open trajectories and the two Potts dimensions satisfy the sum rule<sup>32</sup>

$$d = 2D_C - D - \vartheta, \quad (118)$$

with  $d = 2$  the dimension of the spacetime box. With  $D$  and  $D_C$  known exactly, the expression for  $\vartheta$  follows.

Finally, the expression for the exponent  $\sigma$  can be inferred from the values  $\sigma = 1$  for  $N \rightarrow 0$  ( $\bar{\kappa} = \frac{2}{3}$ ) and  $\sigma = 0$  for  $N = 2$  ( $\bar{\kappa} = 1$ ). This last value reflects the special status of the XY model, undergoing a phase transition of the Berezinskii-Kosterlitz-Thouless type characterized by algebraic long-range order.<sup>55,56</sup> Assuming, as is the case for Fortuin-Kasteleyn clusters, that both  $\tau$  and  $\sigma$  have a similar dependence on  $\bar{\kappa}$ , we deduce that  $\sigma = 8(1 - \bar{\kappa})/(2 + \bar{\kappa})$ .

To sum up this subsection, the two configurational entropy exponents  $\tau$  (loops) and  $\vartheta$  (open worldlines), and  $\sigma$  for the  $O(N)$  model with  $-2 \leq N \leq 2$  are given in terms of  $\bar{\kappa}$  by

$$\tau = \frac{6 + \bar{\kappa}}{2 + \bar{\kappa}}, \quad \vartheta = -1 + \frac{\bar{\kappa}}{2} + \frac{3}{4} \frac{1}{\bar{\kappa}}, \quad \sigma = 8 \frac{1 - \bar{\kappa}}{2 + \bar{\kappa}}. \quad (119)$$

Table 1 collects the resulting values for the various two-dimensional  $O(N)$  models together with the corresponding thermal critical exponents. It is worth pointing out that for  $N = -2$  indeed Gaussian exponents are obtained, but that the fractal dimension of the high-temperature graphs is not given by that of a Brownian random walk, which has  $D = 2$ . Also note that with increasing  $N$ , the exponent  $\vartheta$  decreases, while at the same time the fractal dimension  $D$  increases. The ratio  $\vartheta/D$  appearing in the scaling relation (98) thus decreases with increasing  $N$ , implying that the number of possible rooted open paths with no constraint on their endpoints increases less rapidly with the number of steps  $b$  for larger  $N$ .

### 3.6. Summary

It was shown that the worldlines or high-temperature graphs of the  $O(N)$  theory proliferate right at the thermal critical point, and that the entire set of critical exponents can be retrieved from the fractal structure of these line

Table 1. Critical exponents together with the exponents characterizing the high-temperature graphs (worldlines) of various two-dimensional  $O(N)$  models.

Model	$N$	$\bar{\kappa}$	$\alpha$	$\beta$	$\gamma$	$\eta$	$\nu$	$D$	$\tau$	$\vartheta$	$\sigma$
Gaussian	-2	$\frac{1}{2}$	1	0	1	0	$\frac{1}{2}$	$\frac{5}{4}$	$\frac{13}{5}$	$\frac{3}{4}$	$\frac{8}{5}$
SAW	0	$\frac{2}{3}$	$\frac{1}{2}$	$\frac{5}{64}$	$\frac{43}{32}$	$\frac{5}{24}$	$\frac{3}{4}$	$\frac{4}{3}$	$\frac{5}{2}$	$\frac{11}{24}$	1
Ising	1	$\frac{3}{4}$	0	$\frac{1}{8}$	$\frac{7}{4}$	$\frac{1}{4}$	1	$\frac{11}{8}$	$\frac{27}{11}$	$\frac{3}{8}$	$\frac{8}{11}$
XY	2	1	$-\infty$	$\infty$	$\infty$	$\frac{1}{4}$	$\infty$	$\frac{3}{2}$	$\frac{7}{3}$	$\frac{1}{4}$	0

objects. In this way, a purely geometric description of the phase transition in these systems was arrived at.

#### 4. Monte Carlo Simulations

We next discuss a Monte Carlo study of the Ising model on a square lattice we carried out<sup>30</sup> to support the above findings (for a summary of that study, see Ref. [57]). We consider not the original spin formulation of the model, but the high-temperature representation detailed in Sec. 2.5 instead, and examine whether the fractal structure of the high-temperature graphs indeed encodes the thermal critical behavior. We focus exclusively on the graph configurations and use percolation observables to study the fractal properties of the graphs.

Traditionally, high-temperature expansions are carried out exactly up to a given order by enumerating all possible ways graphs up to that order can be embedded in the lattice.<sup>34</sup> We take a different approach and study the high-temperature graphs by means of Monte Carlo methods. The Metropolis algorithm<sup>58</sup> we use involves a local update and for that reason suffers from critical slowing down close to the transition temperature. We have intentionally chosen the local update as it allows for a particular clean implementation of our ideas. The price we pay for this is that we cannot study too large spacetime boxes. The largest lattice we can reasonably study is of linear size  $L = 256$ .

##### 4.1. Plaquette Update

The update algorithm we use in our purely geometric approach of the Ising model directly generates the high-temperature graphs that contribute to the partition function. Specifically, the closed graphs are generated by means of a Metropolis *plaquette* algorithm. A proposed plaquette update resulting

in  $b'$  occupied bonds is accepted with probability

$$p_{\text{HT}} = \begin{cases} K^{b'-b} & \text{if } b' > b \\ 1 & \text{else} \end{cases}, \quad (120)$$

where  $b$  denotes the number of occupied bonds before the update.<sup>58</sup> In the entire temperature range  $0 \leq \beta \leq \infty$ ,  $K = \tanh \beta \leq 1$ . Reflecting the  $\mathbb{Z}_2$  symmetry of the model, all bonds of an accepted plaquette are changed, i.e., those that were occupied become unoccupied and *vice versa* (see Fig. 8). With  $b_{\square}$  denoting the number of bonds on the proposed plaquette already

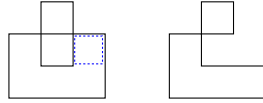


Fig. 8. Plaquette update: An existing high-temperature graph with the plaquette proposed for updating indicated by the broken square (left panel) and the new graph after the proposal is accepted (right panel).

occupied, it follows that

$$b' = b + 4 - 2b_{\square}. \quad (121)$$

The prescription (120) immediately follows from the high-temperature representation (83) of the Ising model. In equilibrium, the probability distribution  $P(G)$  for a given graph configuration  $G$  involving  $b$  occupied bonds reads

$$P(G) = \frac{1}{Z} (\cosh \beta)^{2N} 2^N K^b. \quad (122)$$

Such a configuration can be reached after  $t + 1$  iterations from the configuration present after  $t$  iterations in the following fashion

$$P(G, t + 1) = P(G, t) + \sum_{G'} [P(G', t)W(G' \rightarrow G) - P(G, t)W(G \rightarrow G')], \quad (123)$$

where  $W(G \rightarrow G')$  is the probability for the system to move from the graph configuration  $G$  with  $b$  occupied bonds to the graph configuration  $G'$  with  $b'$  occupied bonds. In equilibrium,  $P(G, t + 1) = P(G, t) = P(G)$ , and the system satisfies detailed balance

$$P(G')W(G' \rightarrow G) = P(G)W(G \rightarrow G'), \quad (124)$$

or

$$\frac{W(G \rightarrow G')}{W(G' \rightarrow G)} = \frac{P(G')}{P(G)} = \frac{K^{b'}}{K^b}. \quad (125)$$

To maximize the acceptance rate of proposed updates, the largest of the two transition probabilities  $W(G \rightarrow G')$  and  $W(G' \rightarrow G)$  appearing in the ratio should be given the largest possible value, i.e., one. Thus, if the number of bonds  $b'$  in the proposed configuration is larger than the number of bonds  $b$  in the present configuration, so that  $K^{b'}/K^b < 1$ , then  $W(G' \rightarrow G) = 1$  and  $W(G \rightarrow G') = p_{\text{HT}}$ . On the other hand, if  $b' < b$ , the proposed configuration carries a larger weight than the present one and will be accepted unconditionally.

By taking plaquettes, i.e., elementary loops on the spacetime lattice as building blocks, the resulting high-temperature graphs are automatically closed (see Fig. 9 for snapshots at three different temperatures).

#### 4.2. Numerical Results

The data was collected on lattices varying in linear size from  $L = 16$  to 256 in  $3.3 \times 10^5$  Monte Carlo sweeps of the lattice close to the critical point and  $1.1 \times 10^5$  sweeps outside the critical region. About 10% of the sweeps were used for equilibration. After each sweep, the resulting graph configuration was analyzed. Statistical errors were estimated by means of binning.

We first determine whether the high-temperature graphs proliferate precisely at the inverse critical temperature  $\beta_c = \ln(1 + \sqrt{2})/2 = 0.440686 \dots$ . (Remember that the inverse temperature is related to the tuning parameter  $K$  via  $K = \tanh \beta$ .) To this end, we measure the so-called spanning probability  $P_S$  as a function of  $\beta$  for different lattice sizes. Giving the probability for the presence of a graph spanning the lattice,  $P_S$  tends to zero for small  $\beta$ , while it tends to unity for large  $\beta$ . This observable has no scaling dimension and plays the role of the Binder cumulant in standard thermodynamic studies. When plotted as a function of  $\beta$ , the curves  $P_S(\beta)$  obtained for different lattice sizes should all intersect in one point. Being independent of the lattice size, this common point marks the proliferation temperature of the *infinite* system. Within the achieved accuracy, we observe that all the measured curves cross at the thermal critical point, implying that the high-temperature graphs loose their line tension  $\theta$  and proliferate precisely at the Curie point (see Fig. 10).

According to standard finite-size scaling, this observable obeys the scal-

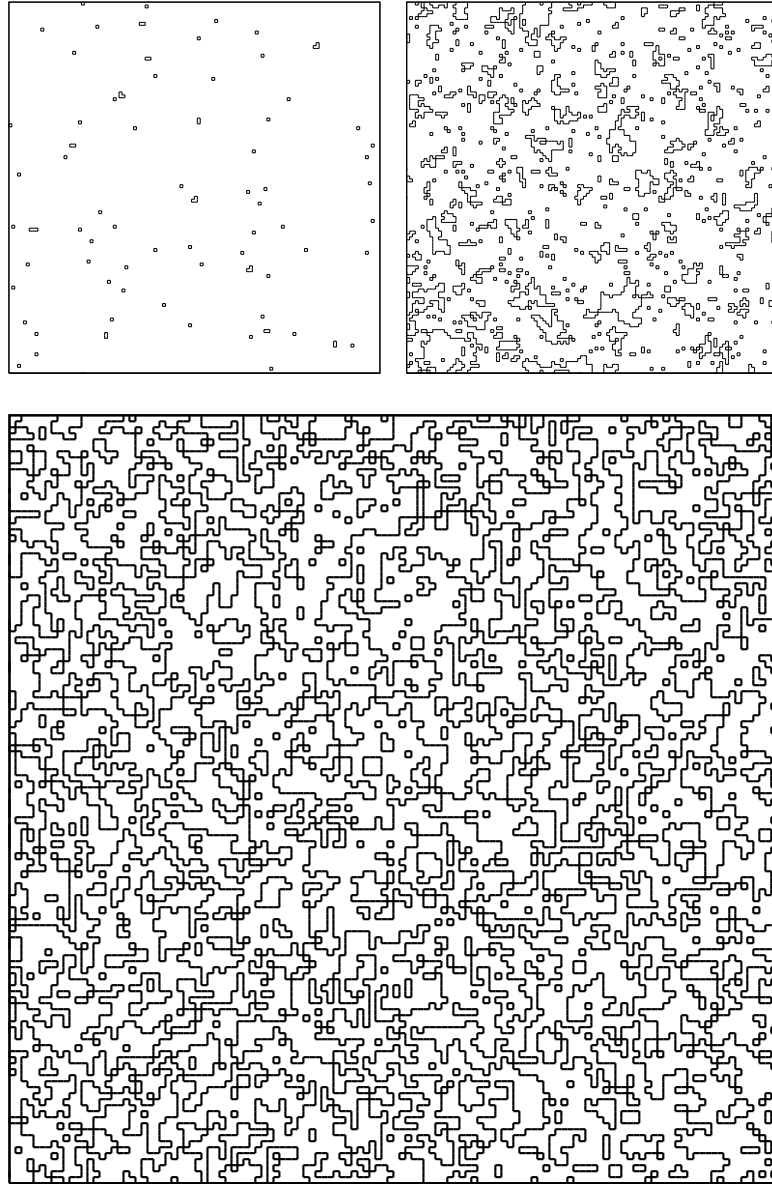


Fig. 9. Snapshots of high-temperature graphs of the Ising model on a square lattice with linear size  $L = 128$  and periodic boundary conditions in the normal phase at  $\beta = 0.6\beta_c$  (top left panel), at the critical point  $\beta = \beta_c$  (top right panel), and in the condensed phase at  $\beta = 1.4\beta_c$  (bottom panel). Because of its richer structure, the last snapshot is enlarged relative to the first two snapshots.

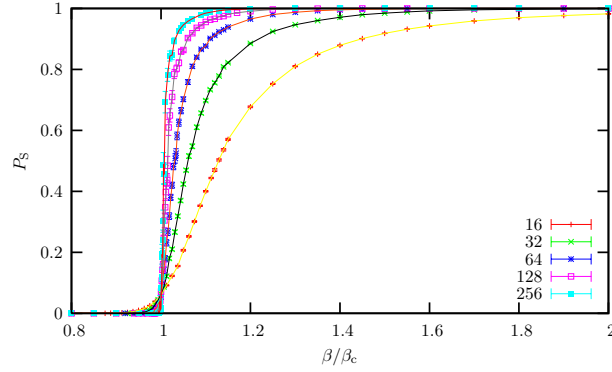


Fig. 10. Probability  $P_S$  for the presence of a spanning graph as function of the inverse temperature  $\beta$  measured for lattice sizes  $L = 16, 32, 64, 128, 256$ . Within the achieved accuracy, the curves cross at the thermal critical point  $\beta = \beta_c$ .

ing law<sup>59</sup>

$$P_S(\beta, L) = P_S(L/\xi), \quad (126)$$

where  $P_S$  is a scaling function and  $\xi$  the correlation length whose divergence at criticality is governed by the exponent  $\nu$ . The data gathered on lattices of different size is therefore a function not of  $\beta$  and  $L$  separately, but only of the ratio of the lattice size and the correlation length. All the data should therefore collapse onto a single curve when plotted as a function of  $(\beta/\beta_c - 1)L^{1/\nu}$ . With  $\nu$  given the Ising value  $\nu = 1$ , this is indeed what we find (see Fig. 11).

The fractal dimension of the high-temperature graphs is best determined by following standard percolation theory<sup>42</sup> and measure the percolation strength  $P_\infty^G$ , defined as the fraction of bonds in the largest graph, and the average graph size  $\chi_G$  (see Figs. 13 and 12). The percolation strength, which is finite in the low-temperature phase ( $\beta > \beta_c$ ), vanishes as a power law when the percolation threshold is approached,

$$P_\infty^G \sim (\beta - \beta_c)^{\beta_G}. \quad (127)$$

At the same time, the average cluster size diverges,

$$\chi_G \sim |\beta - \beta_c|^{-\gamma_G}. \quad (128)$$

Here,  $\beta_G$  and  $\gamma_G$  are two percolation exponents which should not be confused with the thermal critical exponents. The ratios  $\beta_G/\nu$  and  $\gamma_G/\nu$  are

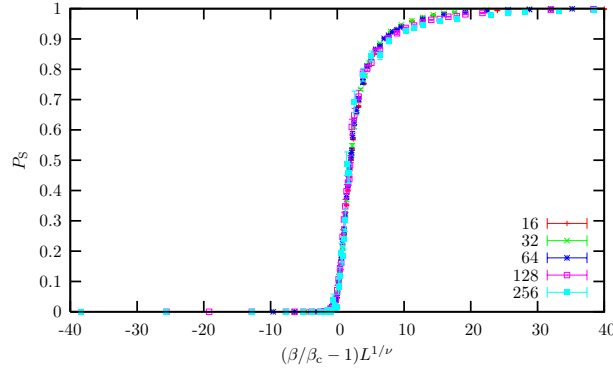


Fig. 11. Raw data of Fig. 10 replotted as a function of  $(\beta/\beta_c - 1)L^{1/\nu}$ , with the Ising choice  $\nu = 1$ . The data collapse is satisfactory over the entire temperature range.

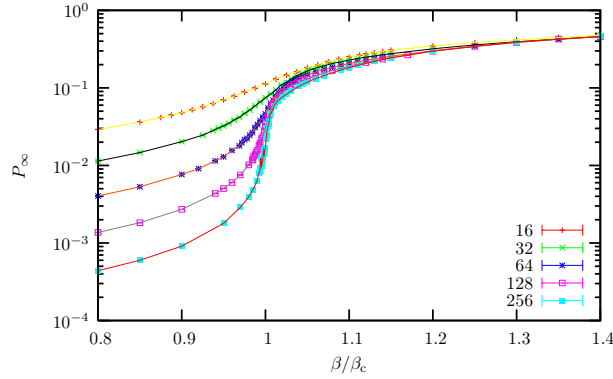


Fig. 12. Percolation strength as a function of the inverse temperature  $\beta$  measured on lattices of linear size  $L = 16, 32, 64, 128, 256$ . Note the logarithmic scale on the vertical axis.

expressed in terms of the entropy exponent  $\tau$  of the graph distribution as in percolation theory<sup>42</sup>

$$\frac{\beta_G}{\nu} = d \frac{\tau - 2}{\tau - 1}, \quad \frac{\gamma_G}{\nu} = d \frac{3 - \tau}{\tau - 1}, \quad (129)$$

with  $d$  the dimensionality of the lattice. According to Table 1,  $\tau = 27/11 = 2.4546\dots$  for the two-dimensional Ising model. Since  $D = d/(\tau - 1)$ , the fractal dimension is related to these percolation exponents via

$$D = d - \frac{\beta_G}{\nu} = \frac{1}{2} \left( d + \frac{\gamma_G}{\nu} \right), \quad (130)$$

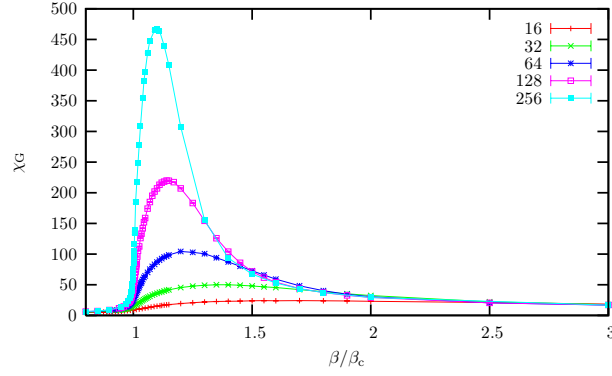


Fig. 13. Average cluster size  $\chi_G$ , excluding the largest cluster, as a function of the inverse temperature measured on lattices of linear size  $L = 16, 32, 64, 128, 256$ .

again as in percolation theory.<sup>42</sup> Close to the percolation threshold, the percolation strength and average graph size obey the finite-size scaling laws

$$P_\infty^G = L^{-\beta_G/\nu} \mathcal{P}_\infty^G(L/\xi), \quad \chi_G = L^{\gamma_G/\nu} \mathcal{X}_G(L/\xi), \quad (131)$$

so that the exponent ratios and thus  $D$  can be determined by considering the system at criticality, where these scaling relations imply an algebraic dependence on the system size  $L$ .

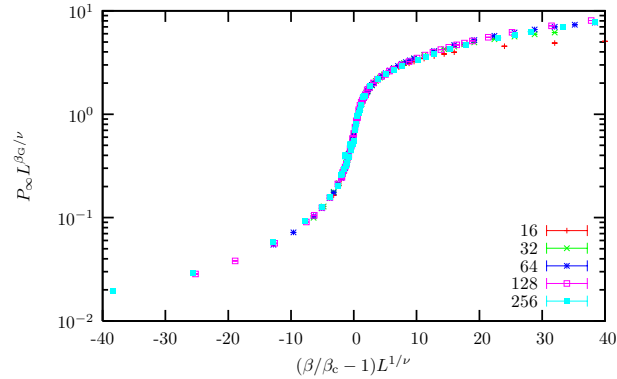


Fig. 14. Rescaled raw data of Fig. 12 plotted as a function of  $(\beta/\beta_c - 1)L^{1/\nu}$ , with the Ising choice  $\nu = 1$ , and  $\beta_G = 0.626$ . The data collapse is satisfactory in the critical region as well as in the entire high-temperature phase  $\beta < \beta_c$ . The flaring out of the data points for  $\beta > \beta_c$  marks the end of the critical region.



We numerically arrived at the estimates<sup>30</sup>  $\beta_G = 0.626(7)$ ,  $\gamma_G = 0.740(4)$ , leading to  $\sigma = 0.732(6)$ ,  $\tau = 2.458(5)$  in perfect agreement with the exact values  $\sigma = 8/11 = 0.7273\dots$ ,  $\tau = 27/11 = 2.4546\dots$ , and the predicted fractal dimension<sup>51</sup>  $D = 11/8$  of the high-temperature graphs. The data were fitted over the range  $L = 16 - 128$ , using the least-squares Marquardt-Levenberg algorithm. With the obtained value for  $\beta_G$ , a satisfactory collapse of the percolation data is achieved (see Fig. 14). The collapse of the average graph size data is less satisfactory. This is not untypical for this type of observable. A similar bad data collapse we observed for the average size of geometrical (as opposed to Fortuin-Kasteleyn) spin clusters in the two-dimensional Ising model.

#### 4.3. Summary

The case study of the Ising model on a square lattice in the high-temperature representation showed that the fractal structure of the high-temperature graphs indeed encodes the thermal critical behavior. This representation therefore provides a purely geometric and equivalent description of the original spin formulation of the model.

### 5. Further Applications

The loop gas approach is by no means limited to the  $O(N)$  theory. The formalism is general and can be applied to a host of other phase transitions, not necessarily involving the proliferation of line objects. Phase transitions involving the proliferation of surfaces and hypersurfaces can be treaded similarly. In this section, a few further applications are briefly discussed.

#### 5.1. Higgs Model

A straightforward extension of the  $O(N)$  theory follows by considering electrically charged particles. The continuum action describing the charged system reads

$$S = \int d^d x \left[ -\frac{1}{2} |(\partial_\mu - ieA_\mu) \varphi|^2 + \frac{m^2}{2} |\varphi|^2 + \frac{g}{4!} |\varphi|^4 + \frac{1}{4} F_{\mu\nu}^2 + \frac{1}{2\alpha} (\partial_\mu A_\mu)^2 \right] \quad (132)$$

where  $F_{\mu\nu} = \partial_\mu A_\nu - \partial_\nu A_\mu$  is the electromagnetic field strength, with  $A_\mu$  the vector potential in  $d$  spacetime dimensions. The scalar field  $\varphi$  is now complex with  $N/2$  complex, i.e.,  $N$  real components, where  $N$  is even. The action is obtained from the neutral theory by minimal coupling the scalar

field to the gauge field  $A_\mu$ , with  $e$  the electric charge. The Maxwell term provides the standard kinetic term for the gauge field, while the last term with parameter  $\alpha$  fixes a Lorentz-invariant gauge. The theory (132) is known as the Abelian Higgs model in high energy and as the Ginzburg-Landau theory in condensed matter physics. The partition function, whose general definition is given in Eq. (1), of the charged theory involves in addition to the functional integral over the scalar field also one over the gauge field, i.e.,

$$\text{Tr} = \int \text{D}\varphi \text{D}A_\mu, \quad (133)$$

where the functional measure  $\int \text{D}\varphi$  is the continuum limit of the discrete measure (4) defined on the spacetime lattice, with an analogous definition for  $\int \text{D}A_\mu$ .

To arrive at the spacetime description of this theory, we concentrate on the coupling to the gauge field by considering only the first two terms in the action,

$$S_0 = \int \text{d}^d x \left[ -\frac{1}{2} |(\partial_\mu - ieA_\mu) \varphi|^2 + \frac{m^2}{2} |\varphi|^2 \right]. \quad (134)$$

This action describes otherwise free particles coupled to an electromagnetic background field, specified by the gauge field  $A_\mu$ . The corresponding partition function

$$\ln Z_0 = \ln \text{Det}^{-N/2} \left[ -(\partial_\mu - ieA_\mu)^2 + m^2 \right] \quad (135)$$

is readily written as a path integral by interpreting the operator  $(\partial_\mu - ieA_\mu)^2 + m^2$  as the Hamiltonian operator of a nonrelativistic charged particle of mass  $M = \frac{1}{2}$  moving in a constant potential  $V = m^2$  in  $d$  dimensions in the presence of an electromagnetic background field. The corresponding classical action is

$$W_0 = \int_0^s \text{d}s' \left\{ \frac{1}{4} \dot{x}^2(s') - ie \dot{x}_\mu A_\mu[x(s')] + m^2 \right\}. \quad (136)$$

According to the mnemonics discussed below Eq. (60), the spacetime representation of the partition function (135) is given in terms of this action as

$$\ln Z_0 = \frac{N}{2} \Omega \int_0^\infty \frac{\text{d}s}{s} \oint \text{D}x(s') e^{-W_0}. \quad (137)$$

Since  $N$  is even here, the simplest Higgs model corresponds to the value  $N = 2$ , which in the context of condensed matter physics provides an effective description of ordinary superconductivity.

It follows from Eq. (137) that a particle trajectory  $\Gamma$  picks up an extra phase factor

$$U(\Gamma) = e^{ie \int_0^s ds' \dot{x}_\mu A_\mu[x(s')]} = e^{ie \int_\Gamma dx_\mu A_\mu(x)}. \quad (138)$$

This phase factor results in a Biot-Savart type of interaction between two line elements  $dx_\mu$ ,  $dy_\nu$  of charged loops<sup>16</sup> as can be illustrated by considering the average of the phase factor (138)

$$\begin{aligned} \langle U(\Gamma) \rangle &\equiv \int DA_\mu U(\Gamma) \exp \left\{ - \int d^d x \left[ \frac{1}{4} F_{\mu\nu}^2 + \frac{1}{2\alpha} (\partial_\mu A_\mu)^2 \right] \right\} \\ &= \exp \left[ - \frac{e^2}{2} \int_\Gamma dx_\mu dy_\nu D_{\mu\nu}(x-y) \right], \end{aligned} \quad (139)$$

where  $D_{\mu\nu}$  is the correlation function of the gauge field

$$D_{\mu\nu}(x) = \int \frac{d^d k}{(2\pi)^d} \frac{1}{k^2} \left[ \delta_{\mu\nu} - (1-\alpha) \frac{k_\mu k_\nu}{k^2} \right] e^{ik \cdot x}, \quad (140)$$

as can be read off from the action (132). This long range Biot-Savart interaction between line elements of charged loops sets the Higgs model apart from the neutral  $O(N)$  theory, where the loops experience only a steric repulsion.

The  $|\varphi|^4$  term in the action (132) can be treated as in the  $O(N)$  theory, leading to a steric repulsion for charged loops. Pasting the pieces together, one arrives at the spacetime representation of the partition function of the Higgs model<sup>19,18,20</sup>

$$\begin{aligned} Z &= \int DA_\mu \exp \left\{ - \int d^d x \left[ \frac{1}{4} F_{\mu\nu}^2 + \frac{1}{2\alpha} (\partial_\mu A_\mu)^2 \right] \right\} \\ &\quad \times \sum_{l=0}^{\infty} \frac{1}{l!} \left( \frac{N}{2} \right)^l \prod_{r=1}^l \left[ \Omega \int_0^\infty \frac{ds_r}{s_r} \oint Dx_r(s'_r) \right] e^{-W^{(l)}}, \end{aligned} \quad (141)$$

with the  $l$ -particle action

$$\begin{aligned} W^{(l)} &= \sum_{r=1}^l \int_0^{s_r} ds'_r \left\{ \frac{1}{4} \dot{x}_r^2(s'_r) + m^2 + ie \dot{x}_{r,\mu}(s'_r) \cdot A_\mu[x_r(s'_r)] \right\} \\ &\quad + \frac{g}{6} \sum_{r,r'=1}^l \int_0^{s_r} ds'_r \int_0^{s_{r'}} ds'_{r'} \delta[x_r(s'_r) - x_{r'}(s'_{r'})]. \end{aligned} \quad (142)$$

The partition function (141) represents a grand canonical ensemble of fluctuating closed worldlines of arbitrary length and shape traced out by electrically charged point particles. Since the matter field  $\varphi$  is complex, the worldlines have an orientation now.

From this spacetime representation it follows that the logarithm of the partition function can again be cast in the general form (87), with the loop distribution now describing charged loops. Because of the additional long range Biot-Savart interaction, the fractal structure of these loops will be different from those featuring in the neutral theory, which experience just a steric repulsion. The physical picture remains unchanged, however. As in the neutral theory, only a few small loops are present in the normal phase due to the finite line tension  $\theta$ . On entering the Higgs phase, characterized by a sign change in the mass term of the Higgs model, the line tension vanishes, and the charged loops proliferate as they can become arbitrary long at no cost. The vacuum becomes filled with “a spaghetti of tangled loops”.<sup>18</sup>

## 5.2. Bose-Einstein Condensation

The spacetime approach was originally formulated to describe nonrelativistic quantum mechanics,<sup>1</sup> which fundamentally differs from its relativistic counterpart. A relativistic quantum particle roams the space dimensions as well as the time dimension, so that its worldlines are random walks in *space-time*. Such particle trajectories are parameterized by the Schwinger proper time parameter, i.e., by their arc length. A nonrelativistic particle, on the other hand, executes a random walk in space only. Its time coordinate is given by absolute Newtonian time, which elapses uniformly forward. In a nonrelativistic ensemble, all the particles execute a random walk in space synchronously in time, with all the worldlines parameterized by Newtonian time. That is, the Schwinger proper time parameter gets replaced by Newtonian time in the nonrelativistic limit. At the technical level, this can be seen by taking the nonrelativistic limit  $c \rightarrow \infty$  in, for example, the correlation function (37) of the relativistic theory. The integral over  $s$  can in this limit be approximated by the saddle point<sup>60</sup>

$$s = \tau/2m, \quad (143)$$

showing that the arc length parameter  $s$  of relativistic worldlines indeed becomes replaced by Newtonian time  $\tau$ . This difference has profound implications. Because Newtonian time always elapses forward, nonrelativistic worldlines can no longer form simple loops on an infinite lattice. As a result, the number of particles present in the system is fixed. On a finite lattice, worldlines still have the possibility to close by wrapping around the lattice.

Figure 15 shows an example of the motion in imaginary time of three particles in one space dimension. Up to now, the finite lattice sizes were

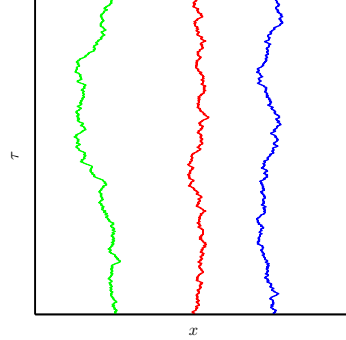


Fig. 15. Worldlines of three nonrelativistic particles on a square lattice, representing one space and the imaginary time dimension, moving synchronously from the bottom to the top of the lattice. The particles execute a Brownian random walk in  $x$ -direction. Periodic boundary conditions are chosen in the imaginary time direction.

considered a mere approximation to systems of infinite extent, in space as well as in time. In this subsection, we instead assume that the imaginary time dimension is finite. With the time variable  $\tau$  restricted to the interval  $0 \leq \tau \leq \hbar\beta$ , with  $\beta$  the inverse temperature  $\beta = 1/k_B T$ , one describes the system at finite temperature. The zero-temperature limit is recovered by letting the imaginary time dimension become infinite. For bosons, periodic boundary conditions are to be imposed in the imaginary time dimension, implying that the configurations of an ensemble of nonrelativistic bosons at imaginary time 0 and at  $\hbar\beta$  are identical. (In contrast to the rest of the paper, we explicitly display factors of  $\hbar$  in this subsection.)

The partition function  $Z_l$  of such an ensemble of  $l$  identical nonrelativistic bosons can be expressed in terms of the probability amplitude  $G[\mathbf{x}(0), \mathbf{x}(\tau)]$  for a particle to move from  $\mathbf{x}(0)$  to  $\mathbf{x}(\tau)$  in imaginary time  $\tau$  as:<sup>61</sup>

$$Z_l = \sum_P \int \prod_{r=1}^l d^d \mathbf{x}_r G[\mathbf{x}_1(0), \mathbf{x}_{P(1)}(\hbar\beta)] \cdots G[\mathbf{x}_l(0), \mathbf{x}_{P(l)}(\hbar\beta)], \quad (144)$$

where the final configuration  $\{\mathbf{x}_{P(r)}(\hbar\beta)\}$  at  $\tau = \hbar\beta$  is a permutation  $P$  of the initial configuration  $\{\mathbf{x}_r(0)\}$  at  $\tau = 0$ . In contrast to the convention used up to now, here,  $d$  denotes the number of *spatial* dimensions. All possible permutations of the starting points are included as indicated by the sum  $\sum_P$ . In Feynman's spacetime approach, the amplitude  $G[\mathbf{x}(0), \mathbf{x}(\tau)]$  is written as a sum over all possible particle trajectories connecting the two

spatial endpoints<sup>1</sup>

$$G[\mathbf{x}(0), \mathbf{x}(\hbar\beta)] = \int D\mathbf{x}(\tau) \exp \left( -\frac{1}{\hbar} \int_0^{\hbar\beta} d\tau \left\{ \frac{m}{2} \dot{\mathbf{x}}^2(\tau) + V[\mathbf{x}(\tau)] \right\} \right), \quad (145)$$

where  $V[\mathbf{x}(\tau)]$  is the potential experienced by the particle along its worldline  $\mathbf{x}(\tau)$ . Expressed as a path integral, the partition function thus reads<sup>15</sup>

$$Z_l = \sum_P \int \prod_{r=1}^l D\mathbf{x}_r(\tau) \exp \left( -\frac{1}{\hbar} \int_0^{\hbar\beta} d\tau L^{(l)} \right) \quad (146)$$

with the  $l$ -particle nonrelativistic Lagrangian

$$L^{(l)} = \sum_{r=1}^l \frac{m}{2} \dot{\mathbf{x}}_r^2(\tau) + \frac{1}{2} \sum_{r \neq r'=1}^l V[|\mathbf{x}_r(\tau) - \mathbf{x}_{r'}(\tau)|] \quad (147)$$

and pair potential  $V(\mathbf{x}_r, \mathbf{x}_{r'}) = V(|\mathbf{x}_r - \mathbf{x}_{r'}|)$ . Figure 15 gives an example of a configuration contributing to  $Z_3$ . Since  $\mathbf{x}_{P(1)}(\hbar\beta) = \mathbf{x}_1(0)$ ,  $\mathbf{x}_{P(2)}(\hbar\beta) = \mathbf{x}_2(0)$ , and  $\mathbf{x}_{P(3)}(\hbar\beta) = \mathbf{x}_3(0)$ , the three particle trajectories form three separate loops around the time axis. This is typical for the high-temperature phase of a nonrelativistic ensemble of bosons, where most particles execute a random walk in space during the time interval  $0 \leq \tau \leq \hbar\beta$  that returns to its initial position. It means that the particles, being distinguishable, behave classically.

By mapping Feynman's spacetime approach onto the problem in classical statistical mechanics of chains of beads connected by springs<sup>62</sup> to numerically evaluate the path integral with the help of the Metropolis Monte Carlo method, Ceperley and Pollock,<sup>63</sup> and others showed that a powerful computational tool emerges that can even accurately describe a strongly interacting system like superfluid  $^4\text{He}$  (for reviews, see Refs. [64, 65]).

Bose-Einstein condensation manifests itself in Feynman's spacetime approach by the formation of so-called *cooperative exchange rings*, where individual particle trajectories hook up to form longer loops.<sup>15</sup> An example is given in Fig. 16. Since  $\mathbf{x}_{P(1)}(\hbar\beta) = \mathbf{x}_2(0)$ ,  $\mathbf{x}_{P(2)}(\hbar\beta) = \mathbf{x}_3(0)$ , and  $\mathbf{x}_{P(3)}(\hbar\beta) = \mathbf{x}_1(0)$ , the three particle trajectories now form a single loop, wrapping the time axis three times. Generally, a particle in a composite exchange ring moves in imaginary time along a trajectory that does not end at its own starting position, but at that of another particle. Whence, although the initial and final configurations are identical, the particles in a composite ring are cyclically permuted. They thereby lose their identity

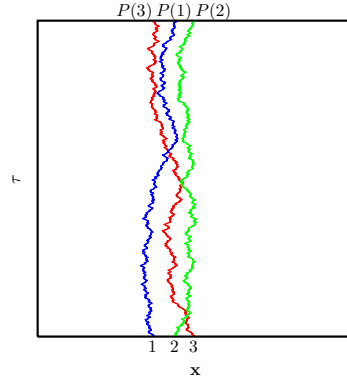


Fig. 16. Worldlines of three nonrelativistic particles on a hypercubic lattice. The vertical direction stands for the imaginary time dimension, while the horizontal direction stands for all the space dimensions. The particles move synchronously from the bottom to the top of the lattice, executing a Brownian random walk in *space*. Periodic boundary conditions are chosen in the time direction. After traversing the lattice, the particles are cyclically permuted  $1 \rightarrow 2 \rightarrow 3 \rightarrow 1$ .

and become indistinguishable. This is the essence of Bose-Einstein condensation, which at finite temperature can occur in space dimensions larger than two.

The connections between geometrical properties and critical exponents spelled out in these notes apply equally well to Bose-Einstein condensation.<sup>27,29</sup> Specifically, the logarithm of the partition function (144) takes close to the condensation temperature again the form (87), with the worldline loop distribution  $\ell_b$  now denoting the number density of worldlines wrapping around the time axis  $b$  times. In the high-temperature phase, the loops have a finite line tension, so that only small loops winding around the imaginary time axis only once or at most a few times exist. Upon approaching the condensation temperature from above, the line tension vanishes and loops with arbitrary large winding numbers appear.<sup>66,27</sup> Since the winding number of a given loop corresponds to the number of cyclically permuted particles in an exchange ring in Feynman's theory, arbitrary large rings appear. The particles contained in large rings (long loops) are part of the condensate.

For a free Bose gas in  $2 < d < 4$  space dimensions,  $\vartheta = 0$  and the fractal dimension of the particle trajectories is that of a Brownian random walk,  $D = 2$ , so that  $\tau = d/2 + 1$ , while  $\sigma = (d - 2)/2$ .<sup>29</sup> Being related to the

thermal critical exponents as before (see Sec. 3.3), these exponents yield

$$\alpha = \frac{d-4}{d-2}, \quad \beta = \frac{1}{2}, \quad \gamma = \frac{2}{d-2}, \quad \nu = \frac{1}{d-2}, \quad \eta = 0, \quad (148)$$

which are precisely the critical exponents of the spherical model in  $d$  space dimensions. This model corresponds to taking the limit  $N \rightarrow \infty$  in the  $O(N)$  spin model.<sup>67,68</sup> Despite being noninteracting, a free Bose gas is not in the universality class of the Gaussian model. The nontrivial exponents (148) derive from the constraint that the total number of particles is fixed. Without this constraint, which is relevant when considering Bose-Einstein condensation in a free Bose gas at constant pressure, Gaussian exponents follow.<sup>67,68</sup> In four space dimensions, corresponding to the upper critical dimension and above, i.e.,  $d \geq 4$ , the exponents of the spherical and Gaussian models coincide.

The critical properties of Bose-Einstein condensation in an *interacting* nonrelativistic Bose gas are given by the  $N = 2, \varphi^4$  universality class. To state this more concretely, the equilibrium thermal critical properties of Bose-Einstein condensation in such an interacting system in three space dimensions, say, can be computed from the theory (3) with  $d = 3$ , now considered a *classical theory* in three space dimensions. The connection between the nonrelativistic quantum theory and the classical  $O(2)$  model is as follows.

Consider the square end-to-end vector  $[\mathbf{x}_r(\tau) - \mathbf{x}_r(0)]^2$  of the  $r$ th particle. For a free Bose gas, with the partition function (146), its average is readily calculated with the result in  $d$  space dimensions

$$\langle [\mathbf{x}_r(\tau) - \mathbf{x}_r(0)]^2 \rangle = d \frac{\hbar}{m} \tau. \quad (149)$$

This expression shows that the worldlines of free nonrelativistic particles can be interpreted as trajectories traced out in *space* by a random walker taking steps of typical size

$$a = \sqrt{\frac{d}{2\pi}} \lambda_T \quad (150)$$

during each imaginary time interval  $\tau = \hbar\beta$ . Here,  $\lambda_T$  is the de Broglie thermal wavelength

$$\lambda_T \equiv \sqrt{\frac{2\pi\hbar^2\beta}{m}}. \quad (151)$$

The step size of the coarse-grained random walk is small when the thermal wavelength is small, i.e., at high temperatures ( $\beta$  small) and for large



particle masses. These conditions correspond to the classical limit. Bose-Einstein condensation sets in when the step size becomes on the order of the interparticle distance  $1/n^{1/d}$ . Setting  $a = 1/n^{1/d}$  leads to an estimate of the condensation temperature of a free Bose gas

$$k_B T_0 = \frac{2\pi\hbar^2}{m} \left( \frac{n}{\zeta(d/2)} \right)^{2/d}, \quad (152)$$

with  $\zeta$  the Riemann zeta function

$$\zeta(s) = \sum_{l=1}^{\infty} \frac{1}{l^s}, \quad (153)$$

and where the particle number density  $n$  is assumed to be given. If this density is small or if the mass of the particles is large, the condensation temperature is low.

The inclusion of a self-interaction in the free (3+1)-dimensional nonrelativistic quantum field theory changes the fractal structure of the worldlines, as they acquire a steric repulsion now, but leaves the basic picture unchanged. Consider a grand canonical nonrelativistic ensemble

$$Z = \sum_{l=0}^{\infty} \frac{1}{l!} e^{\beta\mu l} Z_l, \quad (154)$$

with  $\mu$  the chemical potential and  $Z_l$  given in Eq. (146). The coarse-grained random walks of the interacting theory in three-dimensional space can be identified with the high-temperature graphs of the three-dimensional O(2) spin model. Each set bond corresponds to a particle wrapping the time axis once. On a cubic lattice, the smallest closed graph involves four bonds, so that translated back to the nonrelativistic quantum theory, exchange rings smaller than four are not visible in the spin model. In the high-temperature phase of the spin model, only a few small high-temperature graphs are present. This reflects the fact that in the nonrelativistic quantum theory most worldlines wrap the imaginary time axis only once and that very few larger exchange rings are present at high temperatures. A large single closed high-temperature graph of  $b$  bonds amounts in the nonrelativistic quantum theory to a large exchange ring involving  $b$  particles. The proliferation of high-temperature graphs in the spin model corresponds in the nonrelativistic quantum theory to the proliferation of worldlines, wrapping arbitrary many times around the imaginary time axis, and signals the onset of Bose-Einstein condensation.

### 5.3. Summary

The formalism developed in these notes is shown to be easily adapted to describe charged systems as well as Bose-Einstein condensation.

## 6. Dual Theories

As was first pointed out by Helfrich and Müller,<sup>69</sup> the high-temperature graphs of  $O(N)$  spin models describe in addition to the particle trajectories at the same time a second set of *physical* lines. In this section, we briefly discuss examples in  $d = 2, 3$  and  $4$ , respectively.

### 6.1. Peierls Domain Walls

Consider the Ising, i.e., the  $O(1)$  model on a square lattice. According to the famous Kramers-Wannier duality,<sup>70</sup> the high-temperature graphs of the model form line-like Peierls *domain walls*,<sup>71</sup> separating geometrical spin clusters of opposite orientation on the dual lattice. Each bond in a high-temperature graph cuts a nearest neighbor pair of anti-parallel spins on the dual lattice in two. The link connecting the two anti-parallel spins on the dual lattice is perpendicular to the high-temperature bond on the original lattice. On an infinite lattice, the Kramers-Wannier duality implies that observables calculated at an inverse temperature  $\beta$  in the original Ising model can be transcribed to those of the dual model at an inverse temperature  $\tilde{\beta}$ . The duality map interchanges the low-temperature and high-temperature phases. The relation between the two temperatures is readily established by noting that an occupied high-temperature bond represents a factor  $K = \tanh \beta$ . The anti-parallel spin pair on the dual lattice, that is cut by the high-temperature bond, carries a Boltzmann weight  $\exp(-2\tilde{\beta})$ , so that<sup>70</sup>

$$\tanh \beta = e^{-2\tilde{\beta}}, \quad (155)$$

or  $\sinh 2\beta = 1/\sinh 2\tilde{\beta}$ . The critical temperature  $\beta_c$  follows from this relation by setting  $\beta = \tilde{\beta}$ , with the result

$$\beta_c = \ln(1 + \sqrt{2})/2 = 0.44068679 \dots \quad (156)$$

By the Kramers-Wannier duality, the fractal dimension of the line-like Peierls domain walls at criticality coincides with the one of the high-temperature graphs, i.e.,  $D = \frac{11}{8}$ .

## 6.2. Vortex Lines

We next consider the three-dimensional  $O(2)$  model. The fractal dimension of the corresponding high-temperature graphs has been estimated in a recent Monte Carlo study<sup>48</sup> as  $D = 1.7655(20)$  at the critical point. By a duality map,<sup>16,17,18</sup> these high-temperature graphs describe at the same time the magnetic vortex lines of the three-dimensional Higgs model (132). Vortices constitute the topological defects of the Higgs model and are line-like in three dimensions. The duality map again interchanges the low-temperature and high-temperature phases of the two models. Given the values<sup>72</sup>  $\eta = 0.0380(4)$  and  $\nu = 0.67155(27)$  of the  $O(2)$  model obtained through Monte Carlo simulations, the relations (107) and (103) lead to the values

$$\tau = 6.2965(60), \quad \vartheta = 0.1965(20), \quad \sigma = 0.8434(13), \quad (157)$$

for the configurational entropy exponents of closed and open magnetic vortices,  $\tau$  and  $\vartheta$ , respectively, and for the exponent  $\sigma$ , characterizing the vanishing of the line tension when the critical point is approached. The estimate for  $\vartheta$  was first given in Ref. [48].

From the perspective of vortices, the phase diagram of the three-dimensional Higgs model is as follows. For convenience, we take the model as effective theory of ordinary type-II superconductors in three space dimensions. Whereas in the superconducting phase only a few small vortex loops are present, the density and size of the loops increase when the temperature rises. Loops of all sizes appear at the critical point, and the vacuum becomes filled with vortex loops. The disordering effect of the proliferating vortices destroys the superconducting phase and drives the phase transition to the normal phase. Because of the Meissner effect, the magnetic interaction is screened in the superconducting phase and vortex line elements experience only a short range interaction which is well approximated by a steric repulsion. This is precisely the type of interaction experienced by the high-temperature graphs of the  $O(2)$  model.

The three-dimensional  $O(2)$  model also possesses vortex lines as topological solutions. In contrast to those in a superconductor, the vortices in a superfluid experience a long range interaction, mediated by the gapless Goldstone mode associated with the spontaneous breaking of the  $O(2)$  symmetry in the  $|\varphi|^4$  theory. The model whose high-temperature graphs describe these vortices is the Higgs model, as follows again from the duality map.<sup>16,17,18</sup> The long range interaction experienced by the high-temperature graphs of the Higgs model is the Biot-Savart interaction discussed in Sec. 5.1. The

duality between the  $O(2)$  and the Higgs models implies that the particle trajectories of one model appear as vortex lines in the other.<sup>18</sup>

It was first suggested by Onsager<sup>73</sup> that proliferating vortex loops drive the superfluid phase transition in liquid  $^4\text{He}$ . He envisaged that as the critical temperature is approached from below, the vortex loops proliferate and thereby disorder the superfluid state, causing the system to revert to the normal state. The precise nature of the three-dimensional superfluid phase transition was recently investigated from this perspective in a recent high-precision Monte Carlo study.<sup>74</sup> One of the observables considered is the total vortex line density  $v$ . By means of standard finite-size scaling analysis of the corresponding susceptibility

$$\chi = L^3(\langle v^2 \rangle - \langle v \rangle^2), \quad (158)$$

the inverse critical temperature  $\beta_c$  was estimated and shown to be consistent with the estimate of a previous study directly in terms of the field variables.<sup>75</sup> However, when percolation observables were considered, such as the probability for the presence of a vortex loop spanning the lattice, slight but statistically significant deviations from  $\beta_c$  were found. For all observables considered, the vortex proliferation threshold  $\beta_p$  is larger than  $\beta_c$ . That is, from these observables one would conclude that the vortices proliferate too early at a temperature below the critical one. From the duality map alluded to above, the vortex proliferation threshold is expected to coincide with the critical point. It is not clear at the moment, whether this discrepancy is physical, or an artifact of the percolation observables used. With the percolation threshold taken as an adjustable parameter, reasonable estimates were obtained from percolation observables for the critical exponents  $\nu$  and  $\beta$ , consistent with those of the XY model.<sup>74</sup>

Even in systems without a thermodynamic phase transition, the notion of vortex proliferation can be useful in understanding the phase structure. An example is provided by the three-dimensional Abelian Higgs lattice model with *compact* gauge field (see below).<sup>76</sup> In addition to vortices, the compact model also features magnetic monopoles as topological defects, which are point-like in three dimensions. In the presence of monopoles, vortex lines no longer need to be closed as they can originate at a monopole and terminate at an antimonopole. When the vortex line tension is finite, monopoles and antimonopoles are tightly bound in pairs. The part of phase diagram where this is the case is called the Higgs region, which corresponds to the superconducting phase in the noncompact theory. When the vortex line tension vanishes, monopoles and antimonopoles are no longer bound

in pairs, and instead form a plasma. In the part of the phase diagram where this is the case, the system exhibits charge confinement. It is well established that one can move from the Higgs region into the confining region without encountering thermodynamic singularities.<sup>77</sup> The susceptibility data for various observables define, however, a precisely located phase boundary. More specifically, for sufficiently large lattices, the maxima of the susceptibilities at the phase boundary do not show any finite-size scaling, and the susceptibility data obtained on different lattice sizes collapse onto single curves without rescaling, indicating that the infinite-volume limit is reached. In Ref. [76], it was argued that this phase boundary marks the vortex proliferation threshold. A well-defined and precisely located phase boundary across which geometrical objects proliferate, yet thermodynamic quantities remain nonsingular has become known as a *Kertész line*. Such a line was first introduced in the context of the Ising model in the presence of an applied magnetic field.<sup>78</sup>

### 6.3. Monopole Loops

As a last example, we consider the four-dimensional *pure compact* U(1) lattice gauge theory described by the Wilson action<sup>79</sup>

$$S_g = \beta \sum_{x, \mu < \nu} [1 - \cos \theta_{x, \mu\nu}]. \quad (159)$$

Here,  $\beta$  is the inverse gauge coupling, the sum extends over all lattice sites  $x$  and lattice directions  $\mu$ , and  $\theta_{x, \mu\nu}$  denotes the plaquette variable

$$\theta_{x, \mu\nu} \equiv \Delta_\mu \theta_{x, \nu} - \Delta_\nu \theta_{x, \mu}, \quad (160)$$

with the lattice difference operator  $\Delta_\nu \theta_{x, \mu} \equiv \theta_{x+a\hat{\nu}, \mu} - \theta_{x, \mu}$  and the compact variable  $\theta_{x, \mu} \in [-\pi, \pi)$ , living on the link connecting the lattice site  $x$  with  $x + a\hat{\mu}$ . The link variable is related to the continuum gauge field  $A_\mu(x)$  via

$$\theta_{x, \mu} = eaA_\mu(x). \quad (161)$$

The lattice action (159) reduces to the ordinary Maxwell action in the continuum limit  $a \rightarrow 0$ , provided one sets

$$\beta = \frac{1}{a^{4-d}e^2}. \quad (162)$$

As for the compact Higgs model, the pure compact gauge theory possesses point-like monopoles in three dimensions. In four dimensions, these defects become line-like.<sup>80</sup> The monopole loops experience in addition to a steric repulsion also a long range Biot-Savart interaction. The field theory in which

these monopole lines appear as particle trajectories (high-temperature graphs) is the four-dimensional noncompact Higgs model (132).<sup>16,17,19</sup> That is, the pure compact U(1) lattice gauge theory is dual to the noncompact Higgs model. These models possess two phases. The pure compact U(1) theory has a confining phase at strong coupling (small  $\beta$ ), corresponding to the superconducting phase of the Higgs model, and a Coulomb phase at weak coupling (large  $\beta$ ) characterized by a massless photon. Monte Carlo simulations<sup>81</sup> show that in the Coulomb phase only a few small monopole loops are present. With increasing coupling constant (decreasing  $\beta$ ), the density and size of the loops increase. At the critical point very close to  $\beta_c = 1.0$ , the monopole loops proliferate and thereby disorder the system.<sup>82,83</sup> The Coulomb phase gives way to the strong-coupling confining phase, where the vacuum is filled with a spaghetti of tangled monopole loops. It is worth emphasizing that the monopole loops drive the phase transition, i.e., the monopole loops proliferate right at the confinement phase transition.<sup>82,83</sup> In showing this, percolation observables of the type discussed here have been used.<sup>24</sup> The order of the phase transition is not an established fact. In case it is continuous, the relations between the fractal structure of loops and the critical exponents laid out in these notes also apply here.

#### 6.4. Summary

Besides picturing the worldlines of the particles described by the field theory under consideration, the high-temperature graphs can have a second interpretation as topological line defects, such as Peierls domains walls ( $d = 2$ ), vortices ( $d = 3$ ), or monopole lines ( $d = 4$ ). The field theory in which such line-like configurations appear as topological defects is said to be dual to the original one. Both field theories describe the same physical lines, once interpreted as particle trajectories, once as line defects.

#### Acknowledgments

One of us (A.S.) kindly thanks Prof. Y. Holovatch for the invitation to present one of the Ising Lectures-2004 at the Institute for Condensed Matter Physics of the National Academy of Sciences, Lviv, Ukraine. He gratefully acknowledges the hospitality and financial support provided by the Institute.

This work is partially supported by the DFG grant No. JA 483/17-3 and by the German-Israel Foundation (GIF) under grant No. I-653-181.14/1999.

## References

1. R. P. Feynman, Rev. Mod. Phys. **20**, 367 (1948).
2. H. Kleinert, *Path Integrals in Quantum Mechanics, Statistics, Polymer Physics, and Financial Markets* (World Scientific, Singapore, 2004) 4th edition.
3. R. P. Feynman, Phys. Rev. **80**, 440 (1950).
4. J. Schwinger, Phys. Rev. **82**, 664 (1951).
5. L. Alvarez-Gaumé and E. Witten in: *Current Algebra and Anomalies*, edited by S. B. Treiman, R. Jackiw, B. Zumino, and E. Witten (World Scientific, Singapore, 1985).
6. A. M. Polyakov, *Gauge Fields and Strings* (Harwood, New York, 1987).
7. M. J. Strassler, Nucl. Phys. B **385**, 145 (1992).
8. C. Schubert, Phys. Rept. **355**, 73 (2001).
9. M. E. Fisher, Rev. Mod. Phys. **70**, 653 (1998).
10. D. J. Amit, *Field Theory, the Renormalization Group and Critical Phenomena* (World Scientific, Singapore, 1984) 2nd edition.
11. D. I. Uzunov, *Introduction to the Theory of Critical Phenomena: Mean Field, Fluctuations and Renormalization* (World Scientific, Singapore, 1993).
12. H. Kleinert and V. Schulte-Frohlinde, *Critical Properties of  $\phi^4$ -Theories* (World Scientific, Singapore, 2001).
13. H. E. Stanley, *Introduction to Phase Transitions and Critical Phenomena* (Oxford University Press, New York, 1971).
14. P. G. de Gennes, Phys. Lett. A **38**, 339 (1972).
15. R. P. Feynman, Phys. Rev. **90**, 1116 (1953); *ibid* **91**, 1291 (1953); *Statistical Mechanics* (Benjamin, Reading, 1972).
16. T. Banks, B. Meyerson, and J. Kogut, Nucl. Phys. B **129**, 493 (1977).
17. M. Peskin, Ann. Phys. **113**, 122 (1978).
18. P. R. Thomas and M. Stone, Nucl. Phys. B **144**, 513 (1978).
19. M. Stone and P. R. Thomas, Phys. Rev. Lett. **41**, 351 (1978).
20. S. Samuel, Nucl. Phys. B **154**, 62 (1979).
21. E. J. Copeland, D. Haws, R. Rivers and S. Holbraad, Physica A **158**, 460 (1989).
22. E. Copeland, D. Haws, S. Holbraad, and R. Rivers, in: *The Formation and Evolution of Cosmic Strings*, edited by G. W. Gibbons, S. W. Hawking, and T. Vachaspati (Cambridge University Press, Cambridge, 1990).
23. A. Patel, Nucl. Phys. B **243**, 411 (1984).
24. S. Hands and R. Wensley, Phys. Rev. Lett. **63**, 2169 (1989).
25. N. D. Antunes, L. M. A. Bettencourt, and M. Hindmarsh, Phys. Rev. Lett. **80**, 908 (1998); N. D. Antunes and L. M. A. Bettencourt, Phys. Rev. Lett. **81**, 3083 (1998).
26. A. K. Nguyen and A. Sudbø, Phys. Rev. B **60**, 15307 (1999).
27. S. Bund and A. M. J. Schakel, Mod. Phys. Lett. B **13**, 349 (1999).
28. J. Hove, S. Mo, and A. Sudbø, Phys. Rev. Lett. **85**, 2368 (2000).
29. A. M. J. Schakel, Phys. Rev. E **63**, 026115 (2001).
30. W. Janke and A. M. J. Schakel, Nucl. Phys. B **700**, 385 (2004).

31. W. Janke and A. M. J. Schakel, Phys. Rev. Lett. **95**, 135702 (2005).
32. W. Janke and A. M. J. Schakel, *Anomalous Scaling and Fractal Dimensions*, cond-mat/0508734 (2005).
33. J. Smit, *Introduction to Quantum Fields on a Lattice* (Cambridge University Press, Cambridge, 2002).
34. H. Kleinert, *Gauge Fields in Condensed Matter* (World Scientific, Singapore, 1989) Vol. 1.
35. J. Ambjørn, Fortschr. Phys. **36**, 595 (1988).
36. K. Symanzik, in *Euclidean Quantum Field Theory*, edited by R. Jost (Academic, New York, 1969).
37. R. Balian and G. Toulouse, Phys. Rev. Lett. **30**, 544 (1973).
38. B. Nienhuis, in: *Phase Transitions and Critical Phenomena*, edited by C. Domb and J. L. Lebowitz (Academic, London, 1987), Vol. 11, p. 1.
39. L. Chayes, L. P. Pryadko, and K. Shtengel, Nucl. Phys. B **570**, 590 (2000).
40. P. R. Gerber and M. E. Fisher, Phys. Rev. B **10**, 4697 (1974).
41. J. L. Jacobsen, N. Read, and H. Saleur, Phys. Rev. Lett. **90**, 090601 (2003).
42. D. Stauffer and A. Aharony, *Introduction to Percolation Theory*, 2nd edition (Taylor & Francis, London, 1994).
43. R. P. Feynman, in: *Progress in Low Temperature Physics*, edited by C. J. Gorter (North-Holland, Amsterdam, 1955), Vol. 1, p. 17.
44. R. H. Swendsen and J. S. Wang, Phys. Rev. Lett. **58**, 86 (1987).
45. U. Wolff, Phys. Rev. Lett. **62**, 361 (1989).
46. K. Binder, Z. Phys. B **43**, 119 (1981).
47. D. S. McKenzie and M. A. Moore, J. Phys. A **4**, L82 (1971).
48. N. Prokof'ev and B. Svistunov, Phys. Rev. Lett. **96**, 219701 (2006).
49. I. Jensen, J. Phys. A **36**, 5731 (2003).
50. I. Jensen, J. Phys. A **37**, 5503 (2004).
51. B. Duplantier and H. Saleur, Phys. Rev. Lett. **61**, 1521 (1988).
52. C. M. Fortuin and P. W. Kasteleyn, Physica **57**, 536 (1972).
53. A. Coniglio, Phys. Rev. Lett. **62**, 3054 (1989).
54. B. Duplantier, Phys. Rev. Lett. **84**, 1363 (2000).
55. V. L. Berezinskii, Sov. Phys. JETP **34**, 610 (1972).
56. J. M. Kosterlitz and D. J. Thouless, J. Phys. **C6**, 1181 (1973).
57. W. Janke and A. M. J. Schakel, Comp. Phys. Comm. **169**, 222 (2005).
58. H.-M. Erking, *A new cluster algorithm for the Ising model*, Diplomarbeit, Technische Universität Graz (2000).
59. K. Binder and D. W. Heermann, *Monte Carlo Simulation in Statistical Physics* (Springer, Berlin, 1997).
60. C. R. Stephens, Ann. Phys. (NY) **181**, 120 (1988).
61. T. Matsubara, Prog. Theor. Phys. **6**, 714 (1951).
62. D. Chandler and P. G. Wolynes, J. Chem. Phys. **74**, 4078 (1981).
63. D. M. Ceperley and E. L. Pollock, Phys. Rev. Lett. **56**, 351 (1986).
64. W. Smith and K. Singer, CCP5 Information Quarterly **25**, 18 (1987).
65. D. M. Ceperley, Rev. Mod. Phys. **67**, 279 (1995).
66. M. Stone, Int. J. Mod. Phys. B **4**, 1465 (1990).
67. J. D. Gunton and M. J. Buckingham, Phys. Rev. **166**, 152 (1968); see also



the textbook: R. K. Pathria, *Statistical Mechanics*, 2nd edition (Butterworth-Heinemann, Oxford, 1996), sec. 12.5.

68. D. V. Shopova and D. I. Uzunov, Phys. Rep. **379**, 1 (2003).
69. W. Helfrich and W. Müller, in *Continuum Models of Discrete Systems* (University of Waterloo Press, Waterloo, Ontario, Canada, 1980) p. 753.
70. H. A. Kramers and G. H. Wannier, Phys. Rev. **60**, 252 (1941).
71. R. Peierls, Proc. Camb. Phil. Soc. **32**, 477 (1936).
72. M. Campostrini, M. Hasenbusch, A. Pelissetto P. Rossi, and E. Vicari, Phys. Rev. B **63**, 214503 (2001).
73. L. Onsager, Nuovo Cimento Suppl. **6**, 249 (1949).
74. E. Bittner, A. Krinner, and W. Janke, Phys. Rev. B **72**, 094511 (2005).
75. E. Bittner and W. Janke, Phys. Rev. Lett. **89**, 130201 (2002); Phys. Rev. B **71**, 024512 (2005).
76. S. Wenzel, E. Bittner, W. Janke, A. M. J. Schakel, and A. Schiller, Phys. Rev. Lett. **95**, 051601 (2005).
77. E. Fradkin and S. H. Shenker, Phys. Rev. D **19**, 3682 (1979).
78. J. Kertész, Physica A **161**, 58 (1989).
79. K. G. Wilson, Phys. Rev. D **10**, 2445 (1974).
80. A. M. Polyakov Phys. Lett. B **59**, 82 (1975).
81. T. A. DeGrand and D. Toussaint, Phys. Rev. D **22**, 2478 (1980).
82. R. Gupta, M. A. Novotny and R. Cordery, Phys. Lett. B **172**, 86 (1986).
83. M. Baig, H. Fort and J. B. Kogut, Phys. Rev. D **50**, 5920 (1994).